

## DETAILED ABUNDANCES FOR 28 METAL-POOR STARS: STELLAR RELICS IN THE MILKY WAY<sup>1,2</sup>

DAVID K. LAI<sup>3</sup>, MICHAEL BOLTE<sup>3</sup>, JENNIFER A. JOHNSON<sup>4</sup>, SARA LUCATELLO<sup>5,6</sup>, ALEXANDER HEGER<sup>3,7</sup>, AND S. E. WOOSLEY<sup>3</sup>

*Draft version October 30, 2018*

### ABSTRACT

We present the results of an abundance analysis for a sample of stars with  $-4 < [\text{Fe}/\text{H}] < -2$ . The data were obtained with the HIRES spectrograph at Keck Observatory. The set includes 28 stars, with effective temperature ranging from 4800 to 6600 K. For 13 stars with  $[\text{Fe}/\text{H}] < -2.6$ , including nine with  $[\text{Fe}/\text{H}] < -3.0$ , and one with  $[\text{Fe}/\text{H}] = -4.0$ , these are the first reported detailed abundances. For the most metal-poor star in our sample, CS 30336-049, we measure an abundance pattern that is very similar to stars in the range  $[\text{Fe}/\text{H}] \sim -3.5$ , including a normal C+N abundance. We also find that it has very low but measurable Sr and Ba, indicating some neutron-capture activity even at this low of a metallicity. We explore this issue further by examining other very neutron-capture-deficient stars, and find that at the lowest levels,  $[\text{Ba}/\text{Sr}]$  exhibits the ratio of the main *r*-process. We also report on a new *r*-process-enhanced star, CS 31078-018. This star has  $[\text{Fe}/\text{H}] = -2.85$ ,  $[\text{Eu}/\text{Fe}] = 1.23$ , and  $[\text{Ba}/\text{Eu}] = -0.51$ . CS 31078-018 exhibits an “actinide boost”, i.e. much higher  $[\text{Th}/\text{Eu}]$  than expected and at a similar level to CS 31082-001. Our spectra allow us to further constrain the abundance scatter at low metallicities, which we then use to fit to the zero-metallicity Type II supernova yields of Heger & Woosley (2008). We find that supernovae with progenitor masses between 10 and 20  $M_{\odot}$  provide the best matches to our abundances.

*Subject headings:* stars: abundances — stars: Population II — supernovae: general — nuclear reactions, nucleosynthesis, abundances

### 1. INTRODUCTION

In recent years the number of discovered extremely metal-poor (EMP,  $[\text{Fe}/\text{H}] \leq -3.0$ ) star candidates has grown substantially, thanks in large part to the survey of Beers et al. (1992), and the more recent Hamburg/ESO (HES) survey (Christlieb et al. 2000). The high-resolution follow-ups to these surveys (e.g. McWilliam et al. 1995; Cohen et al. 2004, 2008; Cayrel et al. 2004; Aoki et al. 2005; Barklem et al. 2005) have verified about 100 stars with  $[\text{Fe}/\text{H}] < -3.0$ .

These EMP stars play an important role in understanding the very first generation of stars (Beers & Christlieb 2005 and references and discussion therein). The lower the metal content of a star, the fewer instances of nucleosynthesis and recycling that preceded its formation. For the most metal-poor stars we may have the opportunity to measure the undiluted imprint of Population III nucleosynthesis. The best examples of this possibility are the two most metal-poor stars known, HE 1327-2326 (Frebel et al. 2005) and HE 0107-5240

(Christlieb et al. 2002). Both stars have  $[\text{Fe}/\text{H}] \sim -5.3$ , and their abundance ratios can be fitted by zero-metallicity supernovae (SNe) with a tuned mixing parameter in the pre-ejecta material (Iwamoto et al. 2005). An alternative scenario to explain the HE 0107-5240 abundance ratios is proposed by Suda et al. (2004), in which it is a Population III star that has accreted its heavy elements through binary and interstellar medium (ISM) accretion. In either case we are most likely seeing the imprint of the first stars, whether it is in SN ejecta or asymptotic giant branch (AGB) evolved material. However, there is a third possibility put forth by Venn & Lambert (2008), that these stars are of a class of chemically peculiar stars that have true  $[\text{Fe}/\text{H}]$  values greater than  $-4.0$ .

As the sample of EMP stars has grown, a curious feature of the metal-poor end of the metallicity distribution function (MDF) of stars in the Galaxy has become apparent. Recently, Norris et al. (2007) discovered a star with  $[\text{Fe}/\text{H}] = -4.8$ , HE 0557-4840, making a total of only three stars with  $[\text{Fe}/\text{H}] < -4.1$ . However, when including these stars in the MDF, as Norris et al. (2007) point out, the number of stars discovered with metallicities  $-5.3 < [\text{Fe}/\text{H}] < -4.1$  still falls 3-4 times short of what is expected from the mixing and fallback models of chemical enrichment (e.g., Salvadori et al. 2007). Instead, a two-component model, as described by Karlsson (2006), where feedback effects from the first massive stars inhibit more star formation, may better fit the statistics of the observed halo MDF.

One key to understanding these issues is to increase the sample of well-studied EMP stars to the point where the different classes of abundance patterns can be identified and therefore explore the nature of their progenitors. While most EMP stars with  $[\text{Fe}/\text{H}] > -3.5$  have relatively small dispersions for elements at or below the iron-peak (e.g. Carretta et al. 2002 and Cayrel et al. 2004), recent observations have shown that there are some objects that are either strongly enhanced or deficient in certain  $\alpha$ -elements

<sup>1</sup> The data presented herein were obtained at the W.M. Keck Observatory, which is operated as a scientific partnership among the California Institute of Technology, the University of California and the National Aeronautics and Space Administration. The Observatory was made possible by the generous financial support of the W.M. Keck Foundation.

<sup>2</sup> This publication makes use of data products from the Two Micron All Sky Survey, which is a joint project of the University of Massachusetts and the Infrared Processing and Analysis Center/California Institute of Technology, funded by the National Aeronautics and Space Administration and the National Science Foundation.

<sup>3</sup> Department of Astronomy and Astrophysics, University of California, Santa Cruz, CA 95064; david@ucolick.org, bolte@ucolick.org, alex@ucolick.org, woosley@ucolick.org.

<sup>4</sup> Department of Astronomy, Ohio State University, 140 W. 18th Ave., Columbus, OH 43210; jaj@astronomy.ohio-state.edu.

<sup>5</sup> Osservatorio Astronomico di Padova, Vicolo dell'Osservatorio 5, 35122 Padua, Italy; sara.lucatello@oapd.inaf.it.

<sup>6</sup> Excellence Cluster Universe, Technische Universität München, D-85748 Garching, Germany.

<sup>7</sup> Theoretical Astrophysics Group, T-6, MS B227, Los Alamos National Laboratory, Los Alamos, NM 87545.

(Aoki et al. 2007 and references therein). At the more metal-poor end, Cohen et al. (2007) report a star with  $[\text{Fe}/\text{H}] \sim -4.0$  and a highly unusual abundance pattern, HE 1424-0241. It has very low  $[\text{Ca}/\text{Fe}]$  and  $[\text{Si}/\text{Fe}]$ ,  $-0.58$  and  $-1.01$ , respectively, but has a  $[\text{Mg}/\text{Fe}]$  of 0.44, which is typical of EMP stars. Cohen et al. (2007) find that there are no core-collapse SN models that can fit this abundance pattern. These important results re-emphasize the need to find more stars in this metallicity regime. Only then can we begin to find out what, if anything, is typical, and it is clear with HE 1424-0241 that we must be very careful extending trends from  $[\text{Fe}/\text{H}] > -3.5$  to lower metallicities.

EMP stars also exhibit a wide dispersion in the ratio of the neutron-capture elements to iron (e.g. McWilliam 1998; Honda et al. 2004; François et al. 2007). By examining both the most neutron-capture rich and neutron capture-poor EMP stars we can shed light on the different processes that give rise to this dispersion. Beginning with the discovery of CS 22892-052 (Sneden et al. 1996, 2003), the imprint of a universal  $r$ -process pattern has been found to stretch from EMP stars up to the Sun. As more  $r$ -process stars are discovered, this result has been even more strongly confirmed (at least for elements with  $Z \geq 56$ ). For the  $s$ -process we are also beginning to see a convergence between observational abundance ratios of the neutron-capture elements in these stars and models of EMP AGB stars (e.g. Johnson & Bolte 2002a, 2004; Masseron et al. 2006). Even though some tuning of the  $^{13}\text{C}$  pocket formation in the AGB star is needed, the match between observed abundances and models is encouraging. These agreements, however, for both the  $r$ -process and  $s$ -process, do not explain the origin of some of the lighter neutron-capture elements ( $Z < 56$ ). To investigate this, the measurement of the light neutron-capture element strontium may prove an ideal probe, as its resonance lines are still detectable in EMP stars. Part of the answer to this puzzle may come from looking at the most neutron-capture poor stars, to isolate the other process(es) that contribute to these elements.

In this study we present abundance ratios from  $[\text{C}/\text{Fe}]$  to  $[\text{Eu}/\text{Fe}]$  for stars in various evolutionary states in the metallicity range  $-4 < [\text{Fe}/\text{H}] < -2$ . In addition to the various nucleosynthesis events described above, mixing that occurs as a star evolves from the main sequence and up the giant branch can also affect the light element abundances up to N (Gratton et al. 2000; Spite et al. 2005, 2006). Our data allows us to both see these evolutionary effects and provide a picture of the early Galaxy through its nucleosynthetic footprint. They also reveal unexpected correlations of  $T_{\text{eff}}$  with Si I, Ti I and Ti II, and Cr I.

In § 2 and § 3 we present the details of the observations and analysis. In § 4 we present the abundance results of our study and compare them to previous samples of metal-poor stars. In § 5 we discuss interesting individual stars, as well as properties of the sample as a whole, including the curious behavior of Si I, Ti I, Ti II, and Cr I. Also in this section we present fits to the zero-metallicity Type II SNe (Sne II) from Heger & Woosley (2008).

## 2. OBSERVATIONS AND REDUCTIONS

We chose our sample from Lai et al. (2004) and metal-poor candidates identified in the photometric sample of Schuster et al. (2004). The data were obtained from multiple runs at the HIRES spectrograph (Vogt et al. 1994) at Keck Observatory between 2001 and 2006. A detector upgrade in mid-2004 allowed us to obtain higher quality spectra in the

blue region. Before the upgrade we typically observed using a blue and red configuration for HIRES, and after the upgrade we observed with a single setup. The details of the observations, including wavelength coverage, signal-to-noise ratio (S/N), and  $V$  magnitude, are given in Table 1.

The reductions were done differently for the data before and after the detector upgrade. The pre-upgrade spectra were reduced with the MAKEE (Mauna Kea Echelle Extraction) reduction package. The post-upgrade data were reduced with the HIRES data reduction package written by J. X. Prochaska.

### 2.1. Equivalent Widths

We used the spectrum analysis code SPECTRE (Fitzpatrick & Sneden 1987) to measure individual equivalent widths (EWs) of isolated lines. The bulk of lines were measured by Gaussian fitting, but for some of the stronger lines we used a Voigt profile to better fit the line wings.

As a check of our accuracy and data quality, we compare our EW measurements with previous high-resolution studies done of common objects. Figure 1 compares the EWs from the studies of Cayrel et al. (2004), Aoki et al. (2005), and Ivans et al. (2003) to our measurements. We share 63 common lines with the Cayrel study for the star BS 16467-062, 438 common lines with the Aoki study from the four stars BS 16080-054, BS 16084-160, CS 30312-059, and CS 30325-028, and 112 common lines with the Ivans study for the stars BD+03 740 and BD+24 1676. As can be seen from the figure, our values are in very good agreement with the three studies. On average we are finding slightly lower EWs than these previous studies of 1.09, 2.41, and 2.24 mÅ, as compared to Cayrel et al. (2004), Aoki et al. (2005), and Ivans et al. (2003), respectively.

## 3. STELLAR PARAMETERS AND ANALYSIS

We used a current version of Turbospectrum (Alvarez & Plez 1998), which properly accounts for continuum scattering (see Cayrel et al. 2004), in combination with the stellar atmospheres from Castelli & Kurucz (2003) to perform LTE line analysis and spectral synthesis. Our atomic line data along with measured EWs are given in Tables 2 through 4. We began with the line lists from Ivans et al. (2006) and Sneden et al. (2003), and added additional lines found using the NIST atomic line database. Specifically we updated/added the following  $gf$ -values: Fe I and Fe II lines with those of Fuhr & Wiese (2006), the Mg lines at 5172.7 and 5183.6 Å with the values from Aldenius et al. (2007), Cr I lines with values from Sobek et al. (2007), Cr II lines with values from Nilsson et al. (2006), the Mn I lines at 3577.9 and 4055.6 Å with values from Blackwell-Whitehead et al. (2005), and Zr II lines with values from Ljung et al. (2006), when available, or otherwise from Malcheva et al. (2006), when available.

To measure oxygen, we adopted the linelist from Kurucz<sup>8</sup> for the OH region at 3185 Å with a dissociation potential of 4.40 eV. We measured nitrogen from the NH feature at 3360 Å. Following the prescription from Johnson et al. (2007) for this list, we used the Kurucz  $gf$ -values divided by 2 with a dissociation potential of 3.45 eV. The CH linelist at 4300 Å was derived from the LIFBASE database (courtesy of B. Plez).

### 3.1. Hyperfine splitting

<sup>8</sup> <http://kurucz.harvard.edu>

The effects of hyperfine splitting (hfs) can greatly affect the derived abundance from strong lines of certain elements. The effect is a desaturation of strong lines, and therefore a larger equivalent width than would be found given the absence of the splitting. Prochaska & McWilliam (2000) noted the effects of hfs for Sc and Mn. We have taken the hfs parameters from Kurucz to account for these two elements. Vanadium and cobalt are also known to be affected by hfs; however, all of our lines are below 20 mÅ, too weak for it to change their derived abundances. We have adopted the hfs parameters and isotope ratios of Ba from McWilliam (1998) along with updated  $gf$ -values used by Ivans et al. (2006). The hfs parameters for Eu are taken from Sneden et al. (2003). The near UV-lines that we use to measure Cu are also known to be greatly affected by hfs (Bihain et al. 2004). We account for this by using the hfs parameters from Kurucz and assuming the solar isotope ratio of  $^{63}\text{Cu}$  to  $^{65}\text{Cu}$  from Anders & Grevesse (1989).

### 3.2. Radial Velocities

Radial velocities were determined by cross-correlating our program star spectra with high-S/N template stars using FXCOR.<sup>9</sup> These template star spectra were taken during the same observing run as the respective program stars, and their radial velocities were measured with individual strong absorption lines (typically 50 lines). These results are given in Table 1. The typical internal error from this procedure is only  $\sim 0.2$  km s<sup>-1</sup>. However this does not take into account the overall zero-point error, particularly given the diversity of our instrument setups. A more realistic estimate to the error in absolute radial velocity can be had by looking at velocities derived for the same object observed during different nights with different instrument setups, but on the same run (i.e. 2004 April 7–9). We find that there is an rms of  $\sim 1.0$  km s<sup>-1</sup> in these measurements. In our sample BS 16084-160 is clearly identified as a radial velocity variable. Also BS 16550-087 is a likely radial velocity variable.

### 3.3. Model Atmosphere Parameters

#### 3.3.1. $T_{\text{eff}}$

We obtained our effective temperatures using the  $V-K$  color of each star. The  $K$  magnitudes were taken from the Two Micron All Sky Survey. We then transformed the color using the updated Alonso et al. (1996, 1999) color- $T_{\text{eff}}$  calibration given by Ramírez & Meléndez (2005). The reddenings were taken from the Schlegel et al. (1998) dust maps, except for values of  $E(B-V)$  greater than 0.10. The Schlegel map may overestimate reddening for higher values (Arce & Goodman 1999); we adopted Equation 1 from Bonifacio et al. (2000) to account for this.

We find a trend in Fe I lines with excitation potential ( $\chi$ ) in many of our stars. This trend is usually accounted for by adjusting the  $T_{\text{eff}}$ . In Table 5 we give the value for the slope of the trends, the corresponding correlation coefficient ( $r$ ), and the number of Fe I lines used, for different cuts on the minimum  $\chi$  considered. Almost all of our stars have a negative slope when considering all Fe I lines, which implies that our  $T_{\text{eff}}$  is too high. Unlike Cohen et al. (2008), we find that using the 0.2 eV cut still leaves a statistically significant cor-

relation between individual Fe I lines and their corresponding  $\chi$ -values. Cayrel et al. (2004) found that a cut at 1.2 eV seemed to eliminate the trends they found, and it does seem to markedly reduce the trends and their statistical significance in this study. However, unlike in Cayrel et al. (2004), small but marginally significant trends still exist. In Figure 2 we show this effect for the above cuts on  $\chi$ .

To test the accuracy of our  $T_{\text{eff}}$  determinations, we also fit the Balmer lines of two of our stars, CS 22880-086 and CS 30336-049. CS 22880-086 in particular shows very little reduction in the trends with the  $\chi$  cuts, and CS 30336-049 has the largest trend with  $\chi$  when considering all Fe I lines. In neither star do we observe  $H\alpha$ , and the  $H\beta$  lines are positioned on the edges of the echelle orders. We therefore fit  $H\gamma$  and  $H\delta$ . For both stars these two Balmer lines are fitted quite well with the  $V-K$ -derived  $T_{\text{eff}}$ . Part of the answer to this discrepancy between spectroscopic temperature with color and Balmer line temperatures may come from the three-dimensional (3D) hydrodynamical effects in these stars. Collet et al. (2007) recently examined the potential impact of this in red giant stars. For metal-poor stars they find a strong effect that would explain the direction of our trend but overestimates the magnitude. For this study we have chosen to stay with the  $V-K$ -derived temperatures and note that the effects of inaccurate  $T_{\text{eff}}$  are minimized by looking at abundance ratios versus absolute abundances.

#### 3.3.2. Surface gravity and Microturbulent velocity

The  $T_{\text{eff}}$  was then used to determine the surface gravity. We used the  $Y^2$  isochrones from Kim et al. (2002), with  $\alpha$ -enhancement set to 0.3 and age to 12 Gyr. We chose not to adjust the log  $g$  spectroscopically to get the abundance of iron from Fe II and Fe I to match. This way we avoid the potential non-LTE (NLTE) effects on the Fe I abundance giving us an erroneous log  $g$ . Even without adjustment our Fe I abundances are in generally very good agreement with the Fe II abundances.

The final microturbulent velocity was determined spectroscopically by eliminating any trend with EW versus abundance for the Fe I lines. Because the  $T_{\text{eff}}$ -color calibration is dependent on metallicity, and therefore the log  $g$  as well, we iterated the above method until we settled on a metallicity within 0.10 dex of our Fe I abundance. The final atmospheric parameters are listed in Table 5. Figure 3 shows the span of evolutionary states of our sample.

#### 3.4. Error Analysis

Excluding systematic NLTE and 1D versus 3D atmosphere effects, the uncertainties in our measurements come from three sources. The first comes from the error in the EW measurement (or in the case of synthesis, the error in the fit). The second comes from errors in the atomic parameters. In most cases we have multiple lines measured for the same element in any given star and the scatter in those lines can give an estimate for the first two error sources. When four or fewer lines of an element in a star are measured, we calculate the average dispersion for the sample in that element, and use this to set a minimum value. We then adopted the larger of the two values, the actual dispersion or this minimum value, to estimate this error component. If there is only a single line measured for a given element, then we assume an error of 0.15 in its abundance. In the case of the synthesis, we estimate this component of the error by how well fitted we can match the synthesis to the actual spectrum (this is typically 0.1).

<sup>9</sup> IRAF is distributed by the National Optical Astronomy Observatories, which are operated by the Association of Universities for Research in Astronomy, Inc., under cooperative agreement with the National Science Foundation.

The third source of error comes from the uncertainty in the model atmosphere parameters. We adopt the errors of 100K and 0.2 dex for  $T_{\text{eff}}$  and  $\log g$ , respectively. The error estimate for  $T_{\text{eff}}$  from using broadband colors has been estimated by multiple authors before (e.g. Cohen et al. 2002), and 100K is a conservative value. The  $\log g$  error is more difficult to estimate. Although we do not use ionization balance to determine surface gravity, as mentioned above we still find that Fe I and Fe II agree very well in our stars. Changes to  $\log g$  of 0.2 dex generally generate a noticeable difference between Fe I and Fe II, and we use this as an error estimate of the isochrones themselves. We estimate the error for microturbulence velocity to be  $0.2 \text{ km s}^{-1}$ , as at differences greater than this pronounced trends of equivalent width versus Fe I line abundances appeared.

We have adopted the error analysis technique described by McWilliam et al. (1995) and Johnson (2002). In particular, we use equations 3, 5, and 6 from Johnson (2002), including the covariance terms to take into account the dependent nature of our  $T_{\text{eff}}$ ,  $\log g$ , and microturbulence values. Because our sample spans a wide range of evolutionary states, we use three different stars to estimate the atmospheric effects, BD+03 740, CS 31078-018, and CS 29502-092, to cover the main-sequence/turnoff, sub- lower giant branch, and the upper giant branch, respectively. In Tables 7, 8, and 9 we summarize the results for these three situations. Using equation 5 and 6 from Johnson (2002), these values can then be used to estimate both the final absolute and relative errors.

### 3.5. Comparison to Previous studies

As a final check of our method and analysis we compare our atmosphere and abundance results to those stars from the studies listed in § 2.1. For BS 16467-062, we also consider additional abundances from Bonifacio et al. (2007) and the abundance analysis by Cohen et al. (2008).

In Table 6 we summarize the atmospheric parameters. In general we are in very good agreement with these previous studies. The agreement with Cohen et al. (2008) is not surprising given that we derive our parameters in a very similar way. All of the other studies, however, use ionization balance to estimate surface gravities. That we agree with these  $\log g$  values adds confidence to the isochrone method that we use to derive surface gravity. One exception to this good agreement is for BD+03 740. Ivans et al. (2003), propose two atmospheres for this star. We have chosen to list in Table 6 the atmosphere that most closely resembles ours. Ivans et al. (2003) go into detail about various other atmosphere and abundance determinations for this object.

We show the abundance comparisons with these studies in Figure 4. In most cases we have good agreement, although there are a few exceptions. We find the largest discrepancy in  $[\text{Al}/\text{Fe}]$  compared to Aoki et al. (2005). The atomic parameters and atmospheres agree quite well between this study and those from Aoki et al. (2005), so those are not the reason for the discrepancy. We believe the disagreement may arise from a CH absorption feature that is blended with the Al  $\lambda 3944$  line.

Another highly discrepant ratio, this time between our study and that of Ivans et al. (2003), is  $[\text{Mn}/\text{Fe}]$ . This difference comes from measured EWs. Ivans et al. (2003) measure only a single Mn I line at  $4823.52 \text{ \AA}$  to have EWs of 14.5 and  $7.3 \text{ m\AA}$  for BD+24 1676 and BD+03 740, respectively. For the same line we measure EWs of 3.0 and  $1.2 \text{ m\AA}$ . We have both

higher S/N and higher resolution spectra than the Ivans et al. (2003) study, and for such low EW lines it is conceivable that their measurements for these two lines were overestimated because of noise. This may also be the cause for the discrepancy we find in  $[\text{Ni}/\text{Fe}]$ . For both objects the common lines are very weak, and we find much lower EWs than Ivans et al. (2003).

## 4. RESULTS

In the following section we discuss our abundance results along with those from various other high-resolution studies. These results are reported in Tables 10 through 15, assuming the solar abundances from Grevesse & Sauval (1998). We comment on the specific elements below, but note that in general the abundances from all of these studies, including our own, agree remarkably well both in trends and in scatter.

### 4.1. The light elements: C, N, O, and Li

Figure 5 shows our values of  $\log\epsilon(\text{Li})$ ,  $[\text{C}/\text{Fe}]$ ,  $[\text{N}/\text{Fe}]$ , and  $[\text{O}/\text{Fe}]$  versus  $[\text{Fe}/\text{H}]$ . Overplotted on each are the values from Spite et al. (2005). For all three elements we find a significant scatter through the whole range of  $[\text{Fe}/\text{H}]$ . In our most metal-poor star, CS 30336-049, we find sub-solar  $[\text{C}/\text{Fe}]$ .

Although we do find similar values of  $[\text{O}/\text{Fe}]$  as Spite et al. (2005), there should be a word of caution in the manner in which we measure  $[\text{O}/\text{Fe}]$ . Spite et al. (2005) use the forbidden O I line at  $6300 \text{ \AA}$ , while we use the UV OH region at  $3185 \text{ \AA}$ . According to Asplund & García Pérez (2001), taking into account 3D effects may reduce oxygen abundances derived from the OH lines by as much as 0.6 dex. However, these models seem to over-predict the solar oxygen abundance derived from helioseismology (Delahaye & Pinsonneault 2006). Because of these uncertainties, we have chosen to present our results without any corrections.

Because of limited wavelength coverage and unfortunate gaps from the pre-upgrade HIRES CCD, we are only able to measure the  $\lambda 6707$  line of lithium for three stars. The lowest metallicity star with a Li abundance is the dwarf CS 22884-108, at  $[\text{Fe}/\text{H}] = -3.13$ , for which we find  $\log\epsilon(\text{Li}) = 2.31$ . The other two measurements are for the stars CS 22872-102 and CS 22878-027, with  $\log\epsilon(\text{Li})$  values of 1.97 and 2.39, respectively. The estimated error for all three measurements is 0.17, and the average value for these three metal-poor dwarfs is 2.21. This agrees very well with the value reported by Bonifacio et al. (2007), whose study of 17 metal-poor dwarfs find an average  $\log\epsilon(\text{Li}) = 2.10$ . In Figure 5, it is clear that our values fall on the Spite plateau, while the giants from Spite et al. (2005) show a significant amount of depletion.

### 4.2. Odd-Z elements: Na, Al, and Sc

In 10 of our stars observed with the original HIRES CCD, our setup allowed us to measure Na from the Na D resonance lines at  $5890$  and  $5895 \text{ \AA}$ , and we were also able to measure Al in all but eight of our stars using one or both of its resonance lines at  $3944$  and  $3961 \text{ \AA}$ . As noted by Cayrel et al. (2004), using these features introduces possible NLTE effects. We report our abundances without NLTE corrections. The suggested NLTE corrections when using these lines are  $-0.5$  for Na (Baumueller et al. 1998) and  $+0.65$  for Al (Baumueller & Gehren 1997).

As can be seen from Figure 6, we do not reproduce the same trend in  $[\text{Na}/\text{Fe}]$  versus  $[\text{Fe}/\text{H}]$  as Cayrel et al. (2004). Although we have fewer measurements of  $[\text{Na}/\text{Fe}]$  in the higher

metallicity range, our data suggest a flat trend in  $[\text{Na}/\text{Fe}]$ . Taken with the Cayrel et al. (2004) points, there appears to be a large scatter in  $[\text{Na}/\text{Fe}]$  down to  $[\text{Fe}/\text{H}] \sim -3.25$ , and then little scatter for lower metallicities.

Figure 6 also shows that our  $[\text{Al}/\text{Fe}]$  abundances agree remarkably well with the Cayrel et al. (2004) and Cohen et al. (2004) distribution of values. In the metallicity range covered by this study, we find a very low 0.12 dex dispersion in  $[\text{Al}/\text{Fe}]$ .

#### 4.3. Alpha elements

The scatter in our  $\alpha$ -elements, as shown in Fig. 7, is very small over the entire range of our metallicities. The rms scatter of these elements is very similar to the value found by previous studies working in our metallicity regime. There are no truly anomalous outliers to the expected  $\alpha$ -enhancement trend (e.g. Aoki et al. 2007; Cohen et al. 2007). This suggests that all of our stars formed from gas produced with a very similar star formation history.

For  $[\text{Mg}/\text{Fe}]$  and  $[\text{Ca}/\text{Fe}]$  the observed scatters are 0.13 and 0.1 with average values of 0.32 and 0.31, respectively. We also find Ti II to be on average 0.09 higher than Ti I. However both the neutral and singly ionized species of Ti show relatively large scatter, about 0.17 dex for both. We caution using this as a sign of true abundance scatter as we find a correlation of Ti with  $T_{\text{eff}}$ . We discuss this further in § 5.2.

Another element that exhibits a large scatter is Si. As we show in Figure 8, we do not find any trends with metallicity and find a rms of 0.24 dex in  $[\text{Si}/\text{Fe}]$ . It appears that part of this scatter comes from a correlation of Si abundance with  $T_{\text{eff}}$  which we also show in Figure 8. This is also discussed further in § 5.2.

#### 4.4. The Fe group ( $23 \leq Z \leq 28$ )

Figure 9 shows the V abundances for our sample. Although we do not measure V I for many of our stars, we do not find an offset between V II and V I as found by Johnson (2002). Overall both the neutral and ionized species give no trend with  $[\text{Fe}/\text{H}]$ , reflecting the similar origins of V and Fe from explosive silicon and oxygen burning (Woosley & Weaver 1995)

In Figure 10, we plot both Cr I and Cr II as a function of  $[\text{Fe}/\text{H}]$ . We reproduce the declining trend of  $[\text{Cr I}/\text{Fe}]$  with  $[\text{Fe}/\text{H}]$  as found in Cayrel et al. (2004) and references therein, albeit with a slightly steeper slope. Although we are only able to measure  $[\text{Cr II}/\text{Fe}]$  for our more metal-rich objects ( $[\text{Fe}/\text{H}] > -3.3$ ), we find a clear offset between the species, with an average  $[\text{Cr II}/\text{Cr I}]$  of 0.22. Furthermore in the metallicity range  $-3.3 < [\text{Fe}/\text{H}] < -2$  that we measure Cr II, we find no evidence for declining  $[\text{Cr II}/\text{Fe}]$  with declining  $[\text{Fe}/\text{H}]$ . We explore this more in § 5.2.

Figure 11 similarly summarizes our Mn abundances. The differences between our study and that of Cayrel et al. (2004) arise from a correction that they chose to adopt for the abundances determined from the Mn I resonance triplet at 4030 Å. They note that in their objects these lines give a consistently lower value ( $\sim 0.4$  dex) for Mn than the non-resonance lines. They therefore do not include them in the final Mn abundance. In the stars where only the triplet lines were detected, their abundance was adopted with a correction of +0.4 dex. We have chosen to include the Mn I triplet in our abundance determinations without correction, since it may have some unknown dependence on the atmospheric parameters of a star (the Cayrel et al. 2004 sample's concentration on giants

avoids this problem). Whatever the cause of this discrepancy, it makes the Mn I abundances suspect. For this reason, we concentrate on the Mn II abundances. In Figure 11 we have also plotted the Mn I abundances from Cayrel et al. (2004) on our Mn II abundances. As can be seen from the figure, our agreement is quite good, although we are finding slightly higher Mn abundances at  $[\text{Fe}/\text{H}] > -3.0$ .

We generally confirm the increase in  $[\text{Co}/\text{Fe}]$  with decreasing  $[\text{Fe}/\text{H}]$  as found by McWilliam et al. (1995) and Cayrel et al. (2004). In Figure 12 we see that the trend matches the points from Cayrel et al. (2004) in general scatter and slope. It is unclear why the points from Cohen et al. (2004) are offset from ours. The line parameters for Co are similar among all three studies. Our  $[\text{Ni}/\text{Fe}]$  values are also shown in this figure, and they stay flat across all metallicities, with a very low rms of 0.10 dex.

#### 4.5. Cu and Zn

In Figure 13, we plot  $[\text{Cu}/\text{Fe}]$  versus  $[\text{Fe}/\text{H}]$  and  $[\text{Zn}/\text{Fe}]$  versus  $[\text{Fe}/\text{H}]$ . It has been known since Sneden & Crocker (1988) that Cu is deficient in metal-poor stars. We are able to extend the  $[\text{Cu}/\text{Fe}]$  measurements down to  $[\text{Fe}/\text{H}] = -4.0$ , comparable to the metallicities of Cohen et al. (2008), and down from the previous low of  $[\text{Fe}/\text{H}] \sim -3.0$  (e.g. Mishenina et al. 2002; Simmerer et al. 2003; Bihain et al. 2004).

The abundance determinations from Cohen et al. (2008) and Bihain et al. (2004) are also shown in the  $[\text{Cu}/\text{Fe}]$  plot. While we find a similar distribution of  $[\text{Cu}/\text{Fe}]$  values as Bihain et al. (2004), Cohen et al. (2008) measure higher  $[\text{Cu}/\text{Fe}]$  abundances. Part of this abundance spread is likely artificial. The version of MOOG used by Cohen et al. (2008), incorrectly treats continuum scattering as absorption. This is properly accounted for in the Turbospectrum code (e.g. Cayrel et al. 2004). We also derived  $[\text{Cu}/\text{Fe}]$  using MOOG and found that those values are on average 0.22 dex higher, with as much as a 0.6 dex difference. Our values are in good agreement with the chemical evolution models of Romano & Matteucci (2007) which assume an initial primary origin of Cu in SNeII, and a secondary contribution from the weak  $s$ -process.

We are only able to measure  $[\text{Zn}/\text{Fe}]$  in a handful of our stars due to gaps in the wavelength coverage of some of our spectra. The values that we are able to measure agree nicely with the results of Cayrel et al. (2004). In particular, our data are consistent with the rise of  $[\text{Zn}/\text{Fe}]$  with decreasing  $[\text{Fe}/\text{H}]$ . Taken together, this rise in  $[\text{Zn}/\text{Fe}]$  could be indicative of an  $\alpha$ -rich freeze out process contributing at a higher level at low metallicities (Cayrel et al. 2004).

#### 4.6. Neutron capture elements

We are able to measure four neutron-capture elements in most of our stars: the light peak elements Sr, Y, and Zr ( $Z=38, 39, \text{ and } 40$ ) and the heavy neutron capture element Ba ( $Z=56$ ). We find a large scatter in these elements relative to Fe, as can be seen in Figure 14.

As found by other studies (e.g., McWilliam et al. 1995; Johnson & Bolte 2002b; Honda et al. 2004; Aoki et al. 2005; François et al. 2007), the light elements also appear to be highly correlated with each other, suggesting that these elements share a common origin. In Figure 15 we show that  $[\text{Y}/\text{Sr}]$  and  $[\text{Zr}/\text{Sr}]$  have consistent values for all stars with their respective averages of  $-0.05$  and  $0.33$ .

The Ba resonance line abundances agree well with the non-resonance lines when measurable, and while we only have three stars with La measurements, these values are roughly consistent with the Ba measurements. The light neutron-capture elements, however, show a remarkable scatter relative to Ba. Figure 15 also shows [Ba/Sr] versus [Fe/H]. The difference between the extreme values is almost 2 dex, replicating the finding of previous work (McWilliam 1998; Johnson & Bolte 2002b; Honda et al. 2004).

We also report on the discovery of a new *r*-process-rich star, CS 31078-018. Table 16 gives the summary of its  $Z \geq 38$  abundances, including thorium. In Figure 16 we show the spectral synthesis of the  $\lambda 4019$  line of Th II, using the  $\log g f$  value measured by Nilsson et al. (2002). For most of the lines used to measure these neutron-capture elements hfs is negligible because of their low EWs ( $< 30$  mÅ). Except for Ba and Eu the only line that is noticeably affected in CS 31078-018 is the resonance line used to measure Yb. To account for this we follow the prescription of Sneden et al. (2003) and use the hfs parameters from Mårtensson-Pendrill et al. (1994).

## 5. DISCUSSION

### 5.1. *Mixing*

For some elements, we expect differences between giants and dwarfs because of internal mixing in giants. Models of mixing and observations of the effect on the abundances in the atmospheres of giants have a long history (e.g., Kraft 1994). The most relevant observations for very metal-poor giants are the Gratton et al. (2000) and Spite et al. (2005) results. The mixing effects can be clearly seen in Figure 17, where we have plotted the light elements (C, N, O, and Li) as a function of  $T_{\text{eff}}$ , where we note that [C/Fe] drops off below  $\sim 5000$ K. We also plot [(C+N)/Fe], which should remain largely unchanged with evolution, as a function of metallicity and  $T_{\text{eff}}$  in Figure 18. There is no correlation of [(C+N)/Fe] with [Fe/H] or with  $T_{\text{eff}}$ , at least for the region for which we have more than upper limits,  $T_{\text{eff}}$  below 5700K.

In Figure 19 we plot  $\log \epsilon(\text{Li})$  as a function of luminosity for our sample as well as those of Gratton et al. (2000) (for [Fe/H]  $< -1.3$ ), Spite et al. (2005), and Bonifacio et al. (2007). We see the clear signature of the deepening convective envelope. The average  $\log \epsilon(\text{Li})$  for the three dwarfs with Li measurements is 2.21, consistent with the Spite plateau value of 2.10 as found by Bonifacio et al. (2007).

### 5.2. *Si, Ti and Cr, unexpected trends with $T_{\text{eff}}$*

Other than for the elements discussed above, mixing processes and therefore the stage of stellar evolution that a star is in should not affect its abundances. However for the Si, Ti, and Cr abundances we do find a correlation of abundance with  $T_{\text{eff}}$ .

We plot our values of [Si/Fe] versus  $T_{\text{eff}}$  in Figure 8. It is clear from this figure that there is a trend of decreasing Si with increasing  $T_{\text{eff}}$ . The Preston et al. (2006) study of field horizontal branch stars and red horizontal branch stars in M15 also suggests this result, and shows that it is not correlated with  $\log g$  as well. This puzzling trend is unexpected from an evolutionary standpoint; the lack of correlation with  $\log g$  shows that it is not tied to mixing along the red giant branch. Preston et al. (2006) carefully checked for contamination from possible CH lines and found very little effect, so that is unlikely the culprit.

We also find a trend of Ti abundance versus  $T_{\text{eff}}$  in the

opposite sense of Si. As we show in Figure 20, this trend shows a decrease in Ti with decreasing  $T_{\text{eff}}$ . In Figure 20 the points from Cayrel et al. (2004) and Cohen et al. (2004) seem to confirm this trend. We have also included the data from Preston et al. (2006) to fill in the sparse region in  $T_{\text{eff}}$  between 5400 and 6000 K. With the inclusion of these horizontal branch stars from Preston et al. (2006), we see that like Si, this is predominately a  $T_{\text{eff}}$ , not  $\log g$  correlation. It also should be noted that this trend applies for both Ti I and Ti II, with respective slopes of 0.12 dex in [Ti I/Fe] per 500K and 0.10 dex in [Ti II/Fe] per 500K.

A similar trend to Ti is found in Cr I. In Figure 21 we plot Cr I and Cr II as a function of  $T_{\text{eff}}$ . A trend of declining [Cr/Fe] with  $T_{\text{eff}}$  can be seen, while [Cr II/Fe] appears, if not flat, then far less pronounced. Again we include data from Preston et al. (2006) in our plots, and we come to the same conclusion that this is a  $T_{\text{eff}}$  and not a  $\log g$  correlation. The slopes of the best fit lines for our data are 0.09 dex in [Cr/Fe] per 500K and only 0.03 dex in [Cr II/Fe] per 500K. This discrepancy in both slope and offset between Cr I and Cr II may point to NLTE effects. This has already been suggested by Sobeck et al. (2007), and the case seems to be made even stronger by our data. Because Cr II appears relatively free of  $T_{\text{eff}}$  trends, we performed a linear fit of [Cr II/Cr I] with  $T_{\text{eff}}$  and suggest that at least as a first step to correct Cr I abundances by this fit. We find that at 6500K, there is an offset of 0.106 dex and a slope of -0.0113 dex per 100 K. This leads to a correction of 0.3 dex at 4800K.

A possible explanation for the observed trends with  $T_{\text{eff}}$  is an incorrect  $T$ - $\tau$  relationship in the adopted model atmospheres, in particular in giants. In fact, the adoption of a  $T$ - $\tau$  relationship shallower than the true one would result in a derived abundance dependent on the depth of the line formation and hence on its strength, with strong lines yielding larger abundance values than weak lines. While this effect on the derived [Fe/H] abundances can be, at least partially, compensated by adjusting the value of the micro-turbulence, this does not apply to Si, Cr and Ti, as the abundances for the first come prevalently from lines forming the outer layers and that for the other two mostly from lines formed deep into the atmosphere. The observed trends could thus be explained in terms of increasing discrepancy between the model atmospheres and the "true" atmospheres at the decreasing of the stellar effective temperature. It is noteworthy that the derived slopes for the  $\chi$ -derived abundance relationship are steeper among giants than among dwarfs (see Table 5), which is what is expected in the hypothesis described.

Whether these are ultimately due to true abundance trends, unaccounted for blends, or a deficiency in our knowledge in the spectral analysis (e.g. NLTE and other atmosphere effects) is yet to be determined. However by including the data from Preston et al. (2006), it seems that this is not an effect of stellar evolution. Regardless, these trends show that caution must be taken when looking at either Ti, Si I or Cr I to explore galactic chemical evolution or to constrain SN models.

### 5.3. *CS 30336-049, [Fe/H]=-4.0*

Of our sample, the star CS 30336-049 is the most metal poor at [Fe/H]=-4.0. There are only three stars more metal-poor than this, and only about seven with comparable metallicities (see Frebel et al. 2007c). It is comparable in metallicity and atmospheric parameters to both CD-38:245 and CS 22949-037 (Cayrel et al. 2004). In its abundance ratios, CS 30336-049 looks far more like CD-38:245 than CS

22949-037. Unlike for CS 22949-037, the derived  $[\text{Mg}/\text{Fe}]$  is actually slightly under-abundant at 0.08 compared to other metal-poor stars. While the high C,N,O and Mg of CS 22949-037 may be suggestive of a low-energy SN explosion (Tsujimoto & Shigeyama 2003), CS 30336-049 is “normal” in all of these abundances except for a high  $[\text{N}/\text{Fe}]$ , leading to a low  $[\text{C}/\text{N}]$  of  $-1.2$ . At the temperature range of this star,  $\sim 4800\text{K}$ , deep mixing may begin to occur and change some of the C to N. Although some of the N then may come from this internal processing in the star, it is possible that much of the low  $[\text{C}/\text{N}]$  value comes from the initial abundances of the cloud that formed the stars. The low carbon abundance of CS 30336-049, coupled with its very low  $[\text{Ba}/\text{Fe}]$  and  $[\text{Sr}/\text{Fe}]$  suggests that the star is not showing mass transferred material from an AGB companion, which suggests a primary source for its enhanced nitrogen abundance.

Just comparing CS 30336-049 with CS 22949-049, it is clear that finding more stars at  $[\text{Fe}/\text{H}]=-4$  is very important. Including HE 1424-0241 as discussed in the introduction, the picture gets even more complicated. If these are all products of one to a small number of SN events, then a census of these objects may provide the best way to constrain the nature of Population III stars. With this in mind, we have attempted to fit our abundances to the recent SN II model yields of Heger & Woosley (2008) in § 5.7.

The low-metallicity of CS 30336-049 also makes it a good candidate for constraining the gas cooling mechanism responsible for the Population III to Population II transition. As noted by Frebel et al. (2007b) and references therein, there are two main competing ideas for this cooling mechanism following the initial metal enrichment from the first stars: atomic fine-structure line cooling and dust-induced fragmentation. Accordingly, Frebel et al. (2007b) define a value they term as the “transition discriminant,”  $D_{\text{trans}}$ , that is dependent on the overall C and O abundance of a star. They find that the cooling from C II and O I fine-structure lines can allow for low-mass star formation only at values of  $D_{\text{trans}} > -3.5 \pm 0.2$ . Intriguingly, CS 30336-049 has a  $D_{\text{trans}}$  value of  $-3.57$ . Given the inherent uncertainty of deriving O from the UV OH lines and the possibility that some C has been converted to N, this is not a highly certain value. However, if this value is correct, then this may be an indication that this star was formed due primarily to fine-structure line cooling from C and O produced from a Population III star. We note that this does not exclude the dust-induced fragmentation model, as even lower abundances of C and O can induce low-mass star formation in this scenario, but that now including CS 30336-049 all metal-poor stars with C and O measurements are consistent with the fine-structure cooling scenario.

#### 5.4. Neutron-capture-poor stars

The existence of stars that are highly neutron-capture element deficient has been known for some time (e.g. McWilliam et al. 1995; Ryan et al. 1996; McWilliam 1998). However these confirmed neutron-capture poor stars are relatively rare. In our own sample, BS 16084-160 and CS 30336-049 are exceptional in their low  $[\text{Sr}/\text{H}]$  and  $[\text{Ba}/\text{H}]$  values. Both of these values for BS 16084-160 agree with those reported by Aoki et al. (2005). Fulbright et al. (2004) analyzed the Draco dSph red giant D119 and found upper limits to  $[\text{Sr}/\text{H}]$  and  $[\text{Ba}/\text{H}]$  that match our values. The recent studies of Cohen et al. (2008), François et al. (2007), Honda et al. (2004), and Aoki et al. (2005) have also added to a handful of stars in this regime. In Table 17 we summarize measure-

ments from recent high-resolution studies for stars with both  $[\text{Ba}/\text{Fe}] < -1.0$  and  $[\text{Ba}/\text{H}] < -4.0$ .

In these neutron-capture element-deficient stars, a striking pattern emerges when comparing  $[\text{Ba}/\text{H}]$  to  $[\text{Sr}/\text{H}]$ . In Figure 22 we can see that there seem to be two populations of stars. Below  $[\text{Ba}/\text{H}] \sim -5.0$ , the Sr and Ba abundances appear to be well coupled. Above this value, however, there is a clear distribution of production of Sr relative to Ba, with the trend of Sr being mainly over-produced relative to Ba. This suggests that the same process, such as a very low-level main  $r$ -process, is producing both the Sr and Ba in the hyper-neutron capture-poor stars (HNCP,  $[\text{Ba}/\text{H}] < -5.0$ ).

To explain the production of Sr without much Ba, leading to high  $[\text{Sr}/\text{Ba}]$  ratios, Qian & Wasserburg (2001) and Travaglio et al. (2004) propose a separation of the process that creates the light (e.g. Sr) and heavy (e.g. Ba) neutron-capture elements (termed the light elementary production process, LEPP, by Travaglio et al. 2004). It has been proposed that the production site for these elements may come from charged-particle reactions in the neutrino driven wind off of a newly born neutron star (Qian & Wasserburg 2007 and references therein). Recently both Montes et al. (2007) and Qian & Wasserburg (2007) explored how a two-component process could account for much of the scatter found in the light to heavy neutron-capture abundances. Figure 22 shows that at the HNCP end this LEPP may somehow be shut off, leaving only the signature of the main  $r$ -process. While there has been much concentration on neutron-capture rich stars, the observational constraints on the production site of the light neutron-capture elements will benefit greatly from more of these HNCP stars being discovered.

#### 5.5. CS 31078-018, A new $r$ -process-rich star

We have discovered a new  $r$ -process-rich star, CS 31078-018. Adopting the categories of Beers & Christlieb (2005), CS 31078-018 is an  $r$ -II star, that is,  $[\text{Eu}/\text{Fe}] > 1$  and  $[\text{Ba}/\text{Eu}] < 0$ . In Figure 23 we plot the neutron-capture abundances of this star over the solar system  $r$ -process abundances taken from Arlandini et al. (1999) and Simmerer et al. (2004).

Similar to previously discovered  $r$ -process-rich stars, the agreement between the solar system  $r$ -process pattern and the abundances for CS 31078-018 is quite good for  $Z \geq 56$ , further strengthening the case for a universal “main”  $r$ -process for the stable neutron-capture elements.

We also find that CS 31078-018 exhibits an “actinide boost.” The Th value is far higher than what should be expected, given its radioactive decay lifetime and the theoretical initial  $r$ -process production ratio. Our measured value of  $\log\epsilon(\text{Th}/\text{Eu}) = -0.19$  gives a negative age for the star if compared to the current estimate of  $-0.28$  for the initial  $r$ -process production ratio (Kratz et al. 2007). This is the third star to exhibit this behavior, after CS 31082-001 (Hill et al. 2002) and CS 30306-132 (Honda et al. 2004).

In Fig. 24 we show the available measurements of  $\log\epsilon(\text{Th}/\text{Eu})$  from the literature for metal-poor stars. There are some clear uncertainties as shown by some of the disagreements between measurements for the same star, but it appears that there is a real distribution of values of  $\log\epsilon(\text{Th}/\text{Eu})$ , with CS 31078-018 near the top. The discrepancy between some of the results from Honda et al. (2004) and other measurements is at least partially explained by differences in their linelist with Westin et al. (2000), and differences in adopted atmospheric parameters with Johnson & Bolte (2001). Qian (2002) proposes a mechanism that allows for a universal  $r$ -

process site for the heavy  $r$ -nuclei but can vary the actinide abundance via neutrino-induced fission, with neutrino exposure being dependent on individual SNe II. A distribution of values may lend credence to the idea of neutrino-induced fission modifying the abundance of thorium. On the other hand, there seems to be an almost bimodal distribution of values, which is even more enhanced if we do not include the values from Honda et al. (2004). This is suggestive of two distinct scenarios with values typified by CS 22892-052 and CS 31078-018. Ultimately more [Th/Eu] measurements will be needed to settle this question.

Regardless of the mechanism that over-produces the actinides in some stars, it is clear from Fig. 24 that it does not affect all  $r$ -process-enhanced stars. Aside from this actinide boost, there is no significant difference between these stars and normal  $r$ -process-enhanced stars, and chronometers based on comparing actinides to these stable elements must be approached with caution.

### 5.6. Abundance Trends and Scatter in the Metal-poor Galaxy

Fig. 25 summarizes the abundance measurements for our entire sample. In the metallicity range that we cover, the only elements to show a trend with [Fe/H] are Cr, Mn, Co, and Cu; our points are consistent with Cayrel et al. (2004) for the trend they find in Zn. These abundance ratio trends are reflected in their larger scatters in Figure 25. As mentioned before, some of the scatter for Cr I may be artificial since we also see a trend with  $T_{\text{eff}}$ , which also can explain why Cayrel et al. (2004) find a much smaller scatter in Cr I as they have a much narrower  $T_{\text{eff}}$  range.

There is a true abundance spread in C and N, although as Figure 18 shows, some of this can be reconciled by considering [(C+N)/Fe] (and therefore evolutionary state) instead. The large scatter in the neutron-capture elements, particularly below [Fe/H] = -3 as shown in Figure 14 is also readily apparent in 25.

What stands out from Figure 25, however is not just the scatter of the previously mentioned elements, but the remarkable consistency in other elements. For example the values for [Ca/Fe], [V/Fe], and [Ni/Fe], given reasonable errors, are effectively the same for all of our stars. This may also be true of [Si/Fe], [Ti/Fe], and [Cr/Fe], but this may be masked by their  $T_{\text{eff}}$  dependence. We are seeing either the evidence of a very well mixed ISM when these stars formed, or evidence that the progenitor stars, possibly Population III stars, were all very similar.

### 5.7. Abundance Pattern fits to zero metallicity SN

If we assume that these early stars were formed from the products of the first stars, then we can try matching them to some of the most up-to-date nucleosynthesis results from zero-metallicity SN explosions. We use the recent models of Heger & Woosley (2008), which are updates to the models of Woosley & Weaver (1995). These models range in mass from 10 to 100  $M_{\odot}$ , energies from 0.3 to 10.0 ( $\times 10^{51}$  ergs), and mixing from none to 0.25. Heger & Woosley (2008) use a 1D code and mixing cannot be followed due to its multi-dimensional nature. Instead, in these models an artificial prescription for this parameter is used from Pinto & Woosley (1988), and the amount of mixing is defined in terms of the mass fraction of the helium core (for a detailed explanation see Heger & Woosley 2008). We then assume that these stars

are the product of one to just a few SN (e.g., Tumlinson 2006b) or assume an IMF of the first stars and match the yield from that to our stars.

We first fit the average abundances of our sample to these models. There are a few general assumptions that we are using to guide us. For all of our fits we are assuming that the Sc and Zn abundances derived from the models are lower limits. It is possible that part of the abundances of both of these elements are synthesized in proton-rich outflows from core-collapse SNe (Pruet et al. 2005), and part of the zinc may also be made in a neutrino-powered wind (Hoffman et al. 1996). Neither of these processes is included in the models of Heger & Woosley (2008). We fit for C+N, instead of C and N separately to account for potential internal cycling, and we ignore O because of possible offsets due to using the OH feature. Finally we have added in the NLTE corrections discussed in § 4.2 to our Na and Al abundances.

We also find a curious result that the models always over-produce copper relative to the observations. In general we ignore copper in our fits, although we discuss it more below. We are also concerned with the trends of Ti, Si, and Cr I discussed in § 5.2, as well as the offset between the neutral and ionized species of Mn. For Ti and Si, we weight their values by only half in the fits compared to the other elements. For Cr and Mn, we choose to use the averages from their ionized species to reduce the impact of potential NLTE effects on their respective neutral species.

In the IMF models the explosion energy of the SN for a star of mass  $M$  is parameterized as

$$E = E_0 \times \left( \frac{M}{20M_{\odot}} \right)^{E^{\text{exp}}} . \quad (1)$$

As a convenient SN energy unit we use bethe,  $1 \text{ B} = 10^{51}$  ergs. Possible values of  $E_0$  in the model database are 0.3, 0.6, 0.9, 1.2, 1.5, 1.8, 2.4, 3.0, 5.0, and 10.0 B, and  $E^{\text{exp}}$  can be -1, -0.5, 0, and 1.

In Figure 26(a) we show the best fit for a Salpeter IMF ( $\Gamma=1.35$ ), for progenitor masses from 10 to 100  $M_{\odot}$  (the entire mass range of the models). In the first case, we assume a standard IMF, where we set  $E^{\text{exp}} = 0$  and  $E_0 = 1.2$ . The only free parameter is the mixing fraction. The fit is actually quite good, returning a standard mixing parameter of 0.16, compared to the canonical value of 0.1 used to explain the light curve of SN1987A (Pinto & Woosley 1988).

We relax the constraints on  $E^{\text{exp}}$  and  $E_0$  in Figure 26(b). We let the energy run over the ranges listed above, and only restrict  $E^{\text{exp}} \geq 0.0$ , and we also let the progenitor lower and upper masses float. The match is noticeably better, with  $\chi^2 = 0.69$  for the best fit model. The  $E_0 = 5.0\text{B}$ , with the explosion energy flat over all masses,  $E^{\text{exp}} = 0.0$ , and no mixing. Also, even though we let the lower and upper bounds of the IMF vary, the best fit still used the entire mass range of models.

Finally in 26(c), we let all the parameters range freely. This now includes letting  $\Gamma$  have the values -0.65, 0.35, 1.35, 2.35, and 3.35, to look at multiple Salpeter-like IMFs. We find a nearly identical fit in terms of  $\chi^2$  with 26(b). The Salpeter power law exponent is still given by  $\Gamma=1.35$ , and the mixing parameter is a low 0.025. The characteristic energy is now much lower with 0.6B, and  $E^{\text{exp}} = -0.50$ . The low explosion energy coupled with the negative value of  $E^{\text{exp}}$  means that we are in effect reducing the importance of high-mass objects. The increased fallback in these objects when the explosion energy is lowered (see Zhang et al. 2008) causes very little of



their metals to be ejected, in particular the innermost Fe-group elements fall back first.

We also constructed Gaussian IMFs to try to match our average abundance distribution. The Gaussians are centered at 11, 12, 13.5, 15, 17, 20, 25, 35, 40, 50, 75, and 100  $M_{\odot}$ . The widths, in  $\log(\text{Mass})$ , range from 0.025 up to 0.5 dex. The energies of the explosions are determined by Eqn. 1, with the same ranges of  $E_0$  and  $E^{\text{exp}}$ . The best-fit Gaussian IMF yield is shown in Fig. 27(a). The fit both looks qualitatively similar to 26(c) and is also quantitatively very similar with a best-fit  $\chi^2 = 0.70$ . This Gaussian IMF is centered at 11.0  $M_{\odot}$ , with a width of 0.3 dex (truncated at 10.0  $M_{\odot}$ ). The energies are defined by  $E^{\text{exp}} = -1.0$  and  $E_0 = 0.6$ , and the mixing is 0.0251. The similarity in the fits is not surprising given that this truncated Gaussian IMF would look very similar to the Salpeter IMF of 26(c). We also fit our average abundance pattern to the entire library of single SN yields. This may be instructive to define a “typical” Population III star, even though clearly this is not the origin of the average abundances. We show the result in Fig. 27(b). The fit is quite good, with a  $\chi^2 = 0.615$ . This best-fit star has a mass of 14.4  $M_{\odot}$ , explosion energy of 1.8B, and a low mixing parameter of 0.015.

We have also performed this best fit analysis on the most metal-poor star of our sample, CS 30336-049. In Figure 28 we show cases similar to those described above, assuming a Salpeter IMF (a), a Gaussian IMF (b), and a single star progenitor (c). We could not measure Cr II in this object, and instead we use the correction to Cr I proposed in § 5.2, and adjust Cr I by +0.3 dex for the fit. Because of the inherent uncertainty of this abundance, we also weight Cr by a factor of 1/2 as is done for Si and Ti. The other assumptions are as detailed in the beginning of this section. The Salpeter IMF has a difficult time fitting the abundance pattern of this star. The fit has a  $\chi^2 = 1.914$ , a very high  $E_0 = 10\text{B}$ ,  $E^{\text{exp}} = -1.0$ ,  $\Gamma = 1.35$ , mixing of 0.025, and ranges over all masses. The Gaussian IMF is best fitted by  $E_0 = 1.2\text{B}$ ,  $E^{\text{exp}} = -1.0$ , a central mass of 11.0  $M_{\odot}$ , a width of 0.225 dex, and mixing of 0.025. The  $\chi^2$  is also a somewhat large 2.40. The most interesting case is the single star fit. The fit is excellent at  $\chi^2 = 0.425$ , with  $M=10.9 M_{\odot}$ ,  $E=0.6\text{B}$ , and a very low mixing parameter of 0.01. This explosion in particular does an excellent job of reproducing the Fe-peak element pattern.

As a final test, we also examined how well different parameters fit our abundances, as opposed to looking only at the single best-fit model. All of the best fits presented above favor progenitor stars with fairly low characteristic masses,  $\sim 10\text{-}15 M_{\odot}$ . The characteristic explosion energies, however, are not as well constrained, with  $E_0$  ranging from 0.6 to 5.0B. The reality is that with so many models that can be compared to (16,800 total), it is relatively easy to find very good fits that are also somewhat degenerate in  $\chi^2$ . With this in mind we show in Figure 29 the best 1000 single SN fits in terms of  $E_0$  and mass both for the average abundance ratio of our sample and for CS 30336-049. The grid-like nature in these plots comes from the discrete values of the models. Overall the results of the best fits from above are borne out. Although in both cases there are a small number of models that have very high explosion energy and mass, the vast majority of fits for our average abundance pattern have masses in between 10 and 20  $M_{\odot}$  and  $E_0$  less than 3.0B, while the results for the abundance pattern of CS 30336-049 show an even narrower range of masses of 10-15  $M_{\odot}$  and typical  $E_0$  less than 1.0B. The mixing parameter could not be constrained with this method

because mass and energy have far greater impact to the fits, and there is not a favored mixing value when looking at the fits in aggregate.

These results seem to fit well with the findings of Tumlinson (2006a), which suggests that the characteristic masses of the first stars were between 8 and 42  $M_{\odot}$ . This is argued from empirical constraints based on the non-detection of Population III stars in the Galactic halo, the Galactic halo MDF, and reionization, not from detailed chemical abundances as done here. As Tumlinson (2006a) notes, these numbers are also close to the results of theoretical models of primordial star formation that incorporate formation feedback effects (e.g. Bromm & Larson 2004 and references therein).

### 5.7.1. Copper, A cautionary note on the choice of explosion mechanism

It is unclear why copper is so over-produced in these models. Part of the solution may come from the choice of these models to locate the piston used to parameterize the explosion at an abrupt entropy jump where the entropy per baryon ( $S/N_A k$ ) is equal to 4, approximately at the base of the convective shell of the pre-SN object. Previously in Woosley & Weaver (1995), it was located where the electron mole number,  $Y_e$ , decreased suddenly, which marked the edge of the iron core.

In Heger & Woosley (2008), there are also a small subset of models with explosion energies of 1.2 and 10 B calculated with the piston located at the  $Y_e$  boundary. To test the effect of the different piston locations, we show in Fig. 30(a) the best-fit single-star model to our average abundances using the  $Y_e$  models (including Cu). This model has a mass of 25.5  $M_{\odot}$ ,  $E_0 = 1.2\text{B}$ , and mixing of 0.1. In 30(b) we show their model with the exact same parameters, but with the piston located at the  $S/N_A k$  boundary. It is clear that the location of the piston can greatly affect the [Cu/Fe]. In the  $Y_e$  model [Cu/Fe] is about -0.70, compared to the approximately solar value found in the same  $S/N_A k$  model. This is not to say which explosion mechanism is correct, as any specification is a parameterized approach, but it does indicate that copper is a less than ideal element to use to constrain current SN models.

## 6. SUMMARY

We have presented the abundances from C to Eu of 28 metal-poor stars covering a wide range of  $T_{\text{eff}}$ . In the process we have found abundance trends with  $T_{\text{eff}}$  of Si I, Ti I and Ti II, and Cr I that may be pointing to the deficiencies of our standard 1-D, LTE spectral analysis, or less likely, an unknown physical process for these elements. In either case the unexplained trends in Si I, Ti, and Cr I with  $T_{\text{eff}}$  show that we must be careful when using them to constrain models of galactic chemical evolution and models of SN yields.

Our sample includes the discovery of a new [Fe/H] = -4.0 star, CS 30336-049. In CS 30336-049, we find abundance ratios that track the trends from more metal-rich objects ([Fe/H]  $\sim -3.5$ ), except for a mildly low [Mg/Fe]. These results for CS 30336-049 show that some of the stars around [Fe/H] = -4.0 have a similar origin to these more metal-rich objects. However, the 10 well-studied stars of similar or lower metallicity show a diversity of abundances far greater than found in the more metal-rich stars.

We have also discovered a new  $r$ -process enhanced star, CS 31078-018. Like other  $r$ -process-enhanced stars, it has a heavy neutron-capture ( $Z > 56$ ) abundance pattern that

matches the scaled solar system  $r$ -process pattern. Interestingly, it has a much higher [Th/Eu] than most other  $r$ -process-rich stars, one that matches the value found in CS 31082-001. From figure 24, it is clear that there is a diversity of [Th/Eu] values in  $r$ -process-rich stars. Whether it is a bimodal distribution or continuous is not yet clear, and it will take more Th measurements to be sorted out. Regardless, it shows that chronometers based solely on this ratio need to be used with caution.

We also explored the origin of the lighter neutron-capture elements ( $Z < 56$ ) by examining stars that are highly deficient in these elements. By using stars in this sample and the literature, we have found that HNCP stars ( $[\text{Ba}/\text{H}] \leq 5$ ) only exhibit the signature of the main  $r$ -process in their [Ba/Sr] abundance. This is in contrast to stars with slightly higher [Ba/H], which show a wide diversity of [Ba/Sr]. This result suggests that if there is a secondary process that produces these lighter elements (i.e. Sr), then it does not operate in the most metal-poor regime. In determining the secondary physical process this may prove to be an important constraint if this continues to hold true as more HNCP stars are found.

Overall, we find very little scatter in our relative abundances for elements in the Fe-group and lighter, and we have largely confirmed many of the trends of abundance with metallicity for stars with  $[\text{Fe}/\text{H}] < -2.0$  that were detailed in Cayrel et al. (2004). The low rms suggests either a well mixed ISM or a common origin for our stars. With this in mind, we have compared the average abundance pattern of our sample with the zero-metallicity SN II nucleosynthesis models

of Heger & Woosley (2008). These fits seem to indicate that metal-free SN II progenitors with masses  $\sim 10\text{-}20 M_{\odot}$  can match our abundances very well. This comparison was also done with the most metal-poor star of our sample, CS 30336-049, where we find that a slightly narrower range of progenitor masses  $\sim 10\text{-}15 M_{\odot}$  give the best matches to its abundance pattern.

D.K.L. would like to acknowledge Chris Sneden, Ruth Peterson, Thomas Masseron, Bob Kraft, and Yong-Zhong Qian for useful discussions, insights, and advice.

D.K.L., M.B., and J.A.J. performed this work with the support of the National Science Foundation (AST-0098617 and AST-0607770).

S.L. performed this work with the support of INAF cofin 2006 and the DFG cluster of excellence ‘‘Origin and Structure of the Universe.’’ S.L. would also like to thank R. Gratton for helpful discussion.

A.H. performed this work under the auspices of the US Department of Energy at the University of California Los Alamos National Laboratory under contract W-7405-ENG-36 and the DOE Program for Scientific Discovery through Advanced Computing (SciDAC; DE-FC02-01ER41176). S.W. received support from the National Science Foundation (AST-02611) and from the DOE SciDAC Program (FC02-06ER41438).

*Facilities:* Keck:I (HIRES)

#### REFERENCES

- Aldenius, M., Tanner, J. D., Johansson, S., Lundberg, H., & Ryan, S. G. 2007, *A&A*, 461, 767
- Alonso, A., Arribas, S., & Martínez-Roger, C. 1996, *A&A*, 313, 873
- Alonso, A., Arribas, S., & Martínez-Roger, C. 1999, *A&AS*, 140, 261
- Alvarez, R., & Plez, B. 1998, *A&A*, 330, 1109
- Anders, E., & Grevesse, N. 1989, *Geochim. Cosmochim. Acta*, 53, 197
- Aoki, W., Honda, S., Beers, T. C., Kajino, T., Ando, H., Norris, J. E., Ryan, S. G., Izumiura, H., Sadakane, K., & Takada-Hidai, M. 2005, *ApJ*, 632, 611
- Aoki, W., Honda, S., Beers, T. C., Takada-Hidai, M., Iwamoto, N., Tominaga, N., Umeda, H., Nomoto, K., Norris, J. E., & Ryan, S. G. 2007, *ApJ*, 660, 747
- Arce, H. G., & Goodman, A. A. 1999, *ApJ*, 512, L135
- Arlandini, C., Käppeler, F., Wisshak, K., Gallino, R., Lugaro, M., Busso, M., & Straniero, O. 1999, *ApJ*, 525, 886
- Asplund, M., & García Pérez, A. E. 2001, *A&A*, 372, 601
- Barklem, P. S., Christlieb, N., Beers, T. C., Hill, V., Bessell, M. S., Holmberg, J., Marsteller, B., Rossi, S., Zickgraf, F.-J., & Reimers, D. 2005, *A&A*, 439, 129
- Baumüller, D., Butler, K., & Gehren, T. 1998, *A&A*, 338, 637
- Baumüller, D., & Gehren, T. 1997, *A&A*, 325, 1088
- Beers, T. C., Chiba, M., Yoshii, Y., Platais, I., Hanson, R. B., Fuchs, B., & Rossi, S. 2000, *AJ*, 119, 2866
- Beers, T. C., & Christlieb, N. 2005, *ARA&A*, 43, 531
- Beers, T. C., Preston, G. W., & Shtetman, S. A. 1992, *AJ*, 103, 1987
- Bihain, G., Israelian, G., Rebolo, R., Bonifacio, P., & Molaro, P. 2004, *A&A*, 423, 777
- Blackwell-Whitehead, R. J., Xu, H. L., Pickering, J. C., Nave, G., & Lundberg, H. 2005, *MNRAS*, 361, 1281
- Bonifacio, P., Molaro, P., Sivarani, T., Cayrel, R., Spite, M., Spite, F., Plez, B., Andersen, J., Barbuy, B., Beers, T. C., Depagne, E., Hill, V., François, P., Nordström, B., & Primas, F. 2007, *A&A*, 462, 851
- Bonifacio, P., Monai, S., & Beers, T. C. 2000, *AJ*, 120, 2065
- Bromm, V., & Larson, R. B. 2004, *ARA&A*, 42, 79
- Carretta, E., Gratton, R., Cohen, J. G., Beers, T. C., & Christlieb, N. 2002, *AJ*, 124, 481
- Castelli, F., & Kurucz, R. L. 2003, in *IAU Symposium*, Vol. 210, *Modelling of Stellar Atmospheres*, ed. N. Piskunov, W. W. Weiss, & D. F. Gray, 20P–+
- Cayrel, R., Depagne, E., Spite, M., Hill, V., Spite, F., François, P., Plez, B., Beers, T., Primas, F., Andersen, J., Barbuy, B., Bonifacio, P., Molaro, P., & Nordström, B. 2004, *A&A*, 416, 1117
- Christlieb, N., Beers, T. C., Barklem, P. S., Bessell, M., Hill, V., Holmberg, J., Korn, A. J., Marsteller, B., Mashonkina, L., Qian, Y.-Z., Rossi, S., Wasserburg, G. J., Zickgraf, F.-J., Kratz, K.-L., Nordström, B., Pfeiffer, B., Rhee, J., & Ryan, S. G. 2004, *A&A*, 428, 1027
- Christlieb, N., Bessell, M. S., Beers, T. C., Gustafsson, B., Korn, A., Barklem, P. S., Karlsson, T., Mizuno-Wiedner, M., & Rossi, S. 2002, *Nature*, 419, 904
- Christlieb, N., Reimers, D., Wisotzki, L., Reetz, J., Gehren, T., & Beers, T. C. 2000, in *The First Stars: Proceedings of the MPA/ESO Workshop Held at Garching, Germany, 4-6 August 1999, ESO ASTROPHYSICS SYMPOSIA*. ISBN 3-540-67222-2. Edited by A. Weiss, T.G. Abel, and V. Hill. Springer-Verlag, 2000, p. 49, ed. A. Weiss, T. G. Abel, & V. Hill, 49–+
- Cohen, J. G., Christlieb, N., Beers, T. C., Gratton, R., & Carretta, E. 2002, *AJ*, 124, 470
- Cohen, J. G., Christlieb, N., McWilliam, A., Shtetman, S., Thompson, I., Melendez, J., Wisotzki, L., & Reimers, D. 2008, *ApJ*, 672, 320
- Cohen, J. G., Christlieb, N., McWilliam, A., Shtetman, S., Thompson, I., Wasserburg, G. J., Ivans, I., Dehn, M., Karlsson, T., & Melendez, J. 2004, *ApJ*, 612, 1107
- Cohen, J. G., McWilliam, A., Christlieb, N., Shtetman, S., Thompson, I., Melendez, J., Wisotzki, L., & Reimers, D. 2007, *ApJ*, 659, L161
- Collet, R., Asplund, M., & Trampedach, R. 2007, *A&A*, 469, 687
- Cowan, J. J., Sneden, C., Burles, S., Ivans, I. I., Beers, T. C., Truran, J. W., Lawler, J. E., Primas, F., Fuller, G. M., Pfeiffer, B., & Kratz, K.-L. 2002, *ApJ*, 572, 861
- Delahaye, F., & Pinsonneault, M. H. 2006, *ApJ*, 649, 529
- Fitzpatrick, M. J., & Sneden, C. 1987, in *Bulletin of the American Astronomical Society*, Vol. 19, *Bulletin of the American Astronomical Society*, 1129–+
- François, P., Depagne, E., Hill, V., Spite, M., Spite, F., Plez, B., Beers, T. C., Andersen, J., James, G., Barbuy, B., Cayrel, R., Bonifacio, P., Molaro, P., Nordström, B., & Primas, F. 2007, *A&A*, 476, 935
- Frebel, A., Aoki, W., Christlieb, N., Ando, H., Asplund, M., Barklem, P. S., Beers, T. C., Eriksson, K., Fechner, C., Fujimoto, M. Y., Honda, S., Kajino, T., Minezaki, T., Nomoto, K., Norris, J. E., Ryan, S. G., Takada-Hidai, M., Tsangarides, S., & Yoshii, Y. 2005, *Nature*, 434, 871
- Frebel, A., Christlieb, N., Norris, J. E., Thom, C., Beers, T. C., & Rhee, J. 2007a, *ApJ*, 660, L117
- Frebel, A., Johnson, J. L., & Bromm, V. 2007b, *MNRAS*, 380, L40
- Frebel, A., Norris, J. E., Aoki, W., Honda, S., Bessell, M. S., Takada-Hidai, M., Beers, T. C., & Christlieb, N. 2007c, *ApJ*, 658, 534
- Fuhr, J. R., & Wiese, W. L. 2006, *Journal of Physical and Chemical Reference Data*, 35, 1669

- Fulbright, J. P., Rich, R. M., & Castro, S. 2004, *ApJ*, 612, 447
- Gratton, R. G., Sneden, C., Carretta, E., & Bragaglia, A. 2000, *A&A*, 354, 169
- Grevesse, N., & Sauval, A. J. 1998, *Space Science Reviews*, 85, 161
- Hauck, B., & Mermilliod, M. 1998, *A&AS*, 129, 431
- Heger, A., & Woosley, S. E. 2008, *ApJ*, submitted (astro-ph/0803.3161)
- Hill, V., Plez, B., Cayrel, R., Beers, T. C., Nordström, B., Andersen, J., Spite, M., Spite, F., Barbuy, B., Bonifacio, P., Depagne, E., François, P., & Primas, F. 2002, *A&A*, 387, 560
- Hoffman, R. D., Woosley, S. E., Fuller, G. M., & Meyer, B. S. 1996, *ApJ*, 460, 478
- Høg, E., Fabricius, C., Makarov, V. V., Urban, S., Corbin, T., Wycoff, G., Bastian, U., Schwekendiek, P., & Wicencenc, A. 2000, *A&A*, 355, L27
- Honda, S., Aoki, W., Kajino, T., Ando, H., Beers, T. C., Izumiura, H., Sadakane, K., & Takada-Hidai, M. 2004, *ApJ*, 607, 474
- Ivans, I. I., Simmerer, J., Sneden, C., Lawler, J. E., Cowan, J. J., Gallino, R., & Bisterzo, S. 2006, *ApJ*, 645, 613
- Ivans, I. I., Sneden, C., James, C. R., Preston, G. W., Fulbright, J. P., Höflich, P. A., Carney, B. W., & Wheeler, J. C. 2003, *ApJ*, 592, 906
- Iwamoto, N., Umeda, H., Tominaga, N., Nomoto, K., & Maeda, K. 2005, *Science*, 309, 451
- Johnson, J. A. 2002, *ApJS*, 139, 219
- Johnson, J. A., & Bolte, M. 2001, *ApJ*, 554, 888
- . 2002a, *ApJ*, 579, L87
- . 2002b, *ApJ*, 579, 616
- . 2004, *ApJ*, 605, 462
- Johnson, J. A., Herwig, F., Beers, T. C., & Christlieb, N. 2007, *ApJ*, 658, 1203
- Karlsson, T. 2006, *ApJ*, 641, L41
- Kim, Y.-C., Demarque, P., Yi, S. K., & Alexander, D. R. 2002, *ApJS*, 143, 499
- Kraft, R. P. 1994, *PASP*, 106, 553
- Kratz, K.-L., Farouqi, K., Pfeiffer, B., Truran, J. W., Sneden, C., & Cowan, J. J. 2007, *ApJ*, 662, 39
- Lai, D. K., Bolte, M., Johnson, J. A., & Lucatello, S. 2004, *AJ*, 128, 2402
- Ljung, G., Nilsson, H., Asplund, M., & Johansson, S. 2006, *A&A*, 456, 1181
- Mårtensson-Pendrill, A.-M., Gough, D. S., & Hannaford, P. 1994, *Phys. Rev. A*, 49, 3351
- Malcheva, G., Blagoev, K., Mayo, R., Ortiz, M., Xu, H. L., Svanberg, S., Quinet, P., & Biéumont, E. 2006, *MNRAS*, 367, 754
- Masseron, T., van Eck, S., Famaey, B., Goriely, S., Plez, B., Siess, L., Beers, T. C., Primas, F., & Jorissen, A. 2006, *A&A*, 455, 1059
- McWilliam, A. 1998, *AJ*, 115, 1640
- McWilliam, A., Preston, G. W., Sneden, C., & Searle, L. 1995, *AJ*, 109, 2757
- Mishenina, T. V., Kovtyukh, V. V., Soubiran, C., Travaglio, C., & Busso, M. 2002, *A&A*, 396, 189
- Montes, F., Beers, T. C., Cowan, J., Elliot, T., Farouqi, K., Gallino, R., Heil, M., Kratz, K., Pfeiffer, B., Pignatari, M., & Schatz, H. 2007, *ArXiv e-prints*, 709
- Nilsson, H., Ljung, G., Lundberg, H., & Nielsen, K. E. 2006, *A&A*, 445, 1165
- Nilsson, H., Zhang, Z. G., Lundberg, H., Johansson, S., & Nordström, B. 2002, *A&A*, 382, 368
- Norris, J. E., Christlieb, N., Korn, A. J., Eriksson, K., Bessell, M. S., Beers, T. C., Wisotzki, L., & Reimers, D. 2007, *ApJ*, 670, 774
- Norris, J. E., Ryan, S. G., & Beers, T. C. 1999, *ApJS*, 123, 639
- Pinto, P. A., & Woosley, S. E. 1988, *Nature*, 333, 534
- Preston, G. W., Sneden, C., Thompson, I. B., Sheckman, S. A., & Burley, G. S. 2006, *AJ*, 132, 85
- Prochaska, J. X., & McWilliam, A. 2000, *ApJ*, 537, L57
- Pruet, J., Woosley, S. E., Buras, R., Janka, H.-T., & Hoffman, R. D. 2005, *ApJ*, 623, 325
- Qian, Y.-Z. 2002, *ApJ*, 569, L103
- Qian, Y.-Z., & Wasserburg, G. J. 2001, *ApJ*, 559, 925
- . 2007, *Phys. Rep.*, 442, 237
- Ramírez, I., & Meléndez, J. 2005, *ApJ*, 626, 465
- Romano, D., & Matteucci, F. 2007, *MNRAS*, 378, L59
- Ryan, S. G., Norris, J. E., & Beers, T. C. 1996, *ApJ*, 471, 254
- Salvadori, S., Schneider, R., & Ferrara, A. 2007, *MNRAS*, 381, 647
- Schlegel, D. J., Finkbeiner, D. P., & Davis, M. 1998, *ApJ*, 500, 525
- Schuster, W. J., Beers, T. C., Michel, R., Nissen, P. E., & García, G. 2004, *A&A*, 422, 527
- Simmerer, J., Sneden, C., Cowan, J. J., Collier, J., Woolf, V. M., & Lawler, J. E. 2004, *ApJ*, 617, 1091
- Simmerer, J., Sneden, C., Ivans, I. I., Kraft, R. P., Shetrone, M. D., & Smith, V. V. 2003, *AJ*, 125, 2018
- Sneden, C., Cowan, J. J., Lawler, J. E., Ivans, I. I., Burles, S., Beers, T. C., Primas, F., Hill, V., Truran, J. W., Fuller, G. M., Pfeiffer, B., & Kratz, K.-L. 2003, *ApJ*, 591, 936
- Sneden, C., & Crocker, D. A. 1988, *ApJ*, 335, 406
- Sneden, C., McWilliam, A., Preston, G. W., Cowan, J. J., Burris, D. L., & Armosky, B. J. 1996, *ApJ*, 467, 819
- Sobeck, J. S., Lawler, J. E., & Sneden, C. 2007, *ApJ*, 667, 1267
- Spite, M., Cayrel, R., Hill, V., Spite, F., François, P., Plez, B., Bonifacio, P., Molaro, P., Depagne, E., Andersen, J., Barbuy, B., Beers, T. C., Nordström, B., & Primas, F. 2006, *A&A*, 455, 291
- Spite, M., Cayrel, R., Plez, B., Hill, V., Spite, F., Depagne, E., François, P., Bonifacio, P., Barbuy, B., Beers, T., Andersen, J., Molaro, P., Nordström, B., & Primas, F. 2005, *A&A*, 430, 655
- Suda, T., Aikawa, M., Machida, M. N., Fujimoto, M. Y., & Iben, I. J. 2004, *ApJ*, 611, 476
- Travaglio, C., Gallino, R., Arnone, E., Cowan, J., Jordan, F., & Sneden, C. 2004, *ApJ*, 601, 864
- Tsujimoto, T., & Shigeyama, T. 2003, *ApJ*, 584, L87
- Tumlinson, J. 2006a, *ApJ*, 641, 1
- . 2006b, *New Astronomy Review*, 50, 101
- Venn, K. A., & Lambert, D. L. 2008, *ApJ*, 677, 572
- Vogt, S. S., Allen, S. L., Bigelow, B. C., Bresee, L., Brown, B., Cantrall, T., Conrad, A., Couture, M., Delaney, C., Epps, H. W., Hilyard, D., Hilyard, D. F., Horn, E., Jern, N., Kanto, D., Keane, M. J., Kibrick, R. I., Lewis, J. W., Osborne, J., Pardeilhian, G. H., Pfister, T., Ricketts, T., Robinson, L. B., Stover, R. J., Tucker, D., Ward, J., & Wei, M. Z. 1994, in Presented at the Society of Photo-Optical Instrumentation Engineers (SPIE) Conference, Vol. 2198, Proc. SPIE Instrumentation in Astronomy VIII, David L. Crawford; Eric R. Craine; Eds., Volume 2198, p. 362, ed. D. L. Crawford & E. R. Craine, 362+
- Westin, J., Sneden, C., Gustafsson, B., & Cowan, J. J. 2000, *ApJ*, 530, 783
- Woosley, S. E., & Weaver, T. A. 1995, *ApJS*, 101, 181
- Zhang, W., Woosley, S. E., & Heger, A. 2008, *ApJ*, 679, 639

TABLE 1  
OBSERVATION DETAILS

Star ID	$V_{mag}$	V Ref.	$v_r$ (km s <sup>-1</sup> )*	Observation Date (UT)	Total Exposure Time (s)	Wavelength Coverage (Å)	S/N 5560 Å	S/N 4500 Å	S/N 3435 Å
BD+03 740	9.80	1	173.1 (0.2)	2004, Oct 7-8	3900	3020-5870	425	340	278
BD+23 3130	8.94	2	-285.1 (0.2)	2006, Aug 19	960	3055-5893	424	245	161
BD+24 1676	10.79	1	-237.8 (0.2)	2004, Oct 7	3600	3020-5870	320	288	193
BS 16077-007	12.41	3	-38.3 (0.2)	2005, May 29-30	2400	3020-5870	142	111	61
BS 16080-054	12.776	4	-121.2 (0.2)	2004, Apr 7	1200	3220-4655	...	78	12
			-119.3 (0.3)	2004, Apr 9	1200	5385-7665	130	...	...
BS 16080-093	13.61	5	-205.2 (0.2)	2001, Aug 25	5400	3770-5280	...	85	...
BS 16084-160	13.14	3	-123.2 (0.2)	2001, Aug 25	7200	3770-5280	...	103	...
			-141.5 (0.2)	2004, Apr 9	1800	5385-7665	140	...	...
			-126.6 (0.2)	2005, May 29	5400	3020-5870	...	111	34
BS 16467-062	14.09	3	-92.4 (0.2)	2003, Jun 6	7200	3770-5280	...	106	...
BS 16545-089	14.44	6	-162.3 (0.2)	2004, Apr 8	9000	3220-4655	...	114	27
			-162.5 (1.0)	2004, Apr 9	3600	5385-7665	100	...	...
BS 16550-087	13.76	7	-144.4 (0.2)	2003, Jun 6	7200	3770-5280	...	65	...
			-148.3 (0.2)	2004, Apr 7	1800	3220-4655	...	63	8
			-148.9 (0.6)	2004, Apr 9	1800	5385-7665	134	...	...
BS 16928-053	13.47	8	-81.5 (0.2)	2004, Apr 7	7200	3220-4655	...	101	11
			-80.9 (0.3)	2004, Apr 9	2700	5385-7665	121	...	...
BS 16929-005	13.61	8	-51.7 (0.2)	2003, Jun 6	1800	3770-5280	...	108	...
			-51.3 (0.2)	2004, Apr 8	7200	3220-4655	...	137	27
			-52.5 (0.5)	2004, Apr 9	2700	5385-7665	117	...	...
CS 22872-102	13.65	3	-59.5 (0.2)	2004, Apr 7	7200	3220-4655	...	138	28
			-56.7 (0.2)	2004, Apr 9	3600	5385-7665	134	...	...
CS 22878-027	14.41	3	-91.5 (0.2)	2004, Apr 8	3600	3220-4655	...	60	13
			-90.1 (0.4)	2004, Apr 9	2700	5385-7665	87	...	...
CS 22880-086	14.41	9	-114.0 (0.2)	2003, Jun 6	7200	3770-5280	...	71	...
CS 22884-108	14.24	3	-18.1 (0.2)	2004, Apr 8	7200	3220-4655	...	93	18
			-18.1 (0.4)	2004, Apr 9	3600	5385-7665	101	...	...
CS 22944-032	13.28	9	17.7 (0.2)	2004, Oct 7-8	7200	3020-5870	212	147	74
CS 22957-022	13.34	3	-33.8 (0.2)	2004, Oct 8	3600	3020-5870	123	95	45
CS 22963-004	14.98	3	292.4 (0.2)	2004, Oct 8	9000	3020-5870	93	71	29
CS 22965-054	15.10	3	-283.0 (0.2)	2001, Aug 25	7200	3770-5280	...	61	...
CS 29502-092	11.895	3	-68.2 (0.2)	2001, Aug 25	5400	3220-4655	...	121	45
			-68.5 (0.2)	2001, Aug 25	5400	3770-5280	...	115	...
			-69.3 (0.2)	2004, Oct 7	4800	3020-5870	253	141	95
CS 29506-007	14.18	3	55.1 (0.2)	2004, Oct 8	5400	3020-5870	85	81	34
CS 29522-046	12.74	3	-106.8 (0.2)	2004, Oct 7-8	5400	3020-5870	185	166	91
CS 30312-059	13.101	4	-156.4 (0.2)	2004, Apr 8	3600	3220-4655	...	134	25
			-155.2 (0.2)	2004, Apr 9	4800	5385-7665	169	...	...
CS 30325-028	12.889	3	-148.8 (0.2)	2005, May 29	5400	3020-5870	146	129	51
CS 30336-049	14.048	3	-237.5 (0.2)	2004, Oct 7-8	7800	3020-5870	94	85	31
CS 31078-018	13.211	7	81.3 (0.2)	2004, Oct 7	7200	3020-5870	167	90	64
CS 31085-024	14.010	3	-322.0 (0.2)	2004, Oct 7-8	9000	3020-5870	150	100	61

REFERENCES. — (1) Hauck & Mermilliod (1998); (2) Høg et al. (2000); (3) Schuster et al. (2004); (4) Aoki et al. (2005); (5) Bonifacio et al. (2000); (6) Cohen et al. (2004); (7) Norris et al. (1999); (8) Honda et al. (2004); (9) Beers et al. (2000)

\* Heliocentric velocity and estimated internal error.

TABLE 2  
EQUIVALENT WIDTHS AND ATOMIC PARAMETERS (FULL VERSION AVAILABLE IN ONLINE EDITION)

Wavelength	Element	$\log gf$	EP	BD+03 740	BD+23 3130	BD+24 1670	BS 16077-007	BS 16080-054	BS 16080-093	BS 16084-160	BS 16545-089	BS 16550-087	BS 16928-053
5889.95	11.0	0.11	0.00	...	128.50	...	...	173.50	...	124.40	25.00	121.00	145.70
5895.92	11.0	-0.19	0.00	...	107.50	...	...	141.00	...	97.70	...	94.50	123.60
3829.36	12.0	-0.21	2.71	...	160.70	...	...	152.40	140.40	136.40	60.40	139.10	144.20
3832.31	12.0	0.15	2.71	...	...	...	...	187.30	167.20	157.70	...	167.10	180.20
4057.52	12.0	-0.90	4.34	6.70	28.60	14.30	...	...	15.50	...	2.00	13.20	...

TABLE 3  
EQUIVALENT WIDTHS AND ATOMIC PARAMETERS (FULL VERSION AVAILABLE IN ONLINE EDITION)

Wavelength	Element	$\log gf$	EP	BS 16929-005	BS 16467-062	CS 22872-102	CS 22878-027	CS 22880-086	CS 22884-108	CS 22944-032	CS 22957-022	CS 22963-004
5889.95	11.0	0.11	0.00	89.60	...	79.50	83.20	...	...	...	...	...
5895.92	11.0	-0.19	0.00	73.30	...	63.90	50.00	...	...	...	...	...
3829.36	12.0	-0.21	2.71	118.30	80.00	...	...	...	79.50	137.90	133.10	96.90
3832.31	12.0	0.15	2.71	...	...	...	...	...	...	...	...	...
4057.52	12.0	-0.90	4.34	11.60	...	9.60	...	...	...	17.10	19.90	...

TABLE 4  
EQUIVALENT WIDTHS AND ATOMIC PARAMETERS (FULL VERSION AVAILABLE IN ONLINE VERSION)

Wavelength	Element	logg	EP	CS 22965-054	CS 29502-092	CS 29506-007	CS 29522-046	CS 30312-059	CS 30325-028	CS 30336-049	CS 31078-018	CS 31085-024
5889.95	11.0	0.11	0.00	...	...	...	...	126.90	...	...	...	...
5895.92	11.0	-0.19	0.00	...	...	...	...	104.90	...	...	...	...
3829.36	12.0	-0.21	2.71	95.40	136.70	...	...	135.90	157.20	83.00	152.00	138.00
3832.31	12.0	0.15	2.71	...	...	...	...	...	...	103.70	...	...
4057.52	12.0	-0.90	4.34	...	18.80	...	46.70	16.40	27.70	...	20.90	11.10

TABLE 5  
STELLAR PARAMETERS

Star ID	[Fe/H]	$T_{\text{eff}}$ (K)	$\log g$ (cgs)	$v_t$ (km s $^{-1}$ )	All lines			$\chi > 0.2\text{eV}$			$\chi > 1.2\text{eV}$		
					$\chi$ trend (dex/eV)	r	Numb. lines	$\chi$ trend (dex/eV)	r	Numb. lines	$\chi$ trend (dex/eV)	r	Numb. lines
BD+03 740	-2.75	6557	4.28	1.8	-0.04	-0.49	102	-0.03	-0.38	91	-0.03	-0.27	76
BD+23 3130	-2.60	5285	2.83	1.6	-0.07	-0.64	150	-0.07	-0.59	133	-0.04	-0.36	107
BD+24 1676	-2.60	6241	3.81	1.6	-0.01	-0.21	119	-0.01	-0.14	107	0.00	-0.02	88
BS 16077-007	-2.80	6544	4.29	1.6	-0.05	-0.56	77	-0.06	-0.54	67	-0.03	-0.29	52
BS 16080-054	-3.00	4805	1.48	2.1	-0.03	-0.29	91	-0.02	-0.05	80	-0.01	-0.05	63
BS 16080-093	-3.20	4940	1.86	1.9	-0.09	-0.69	94	-0.07	-0.52	78	-0.04	-0.23	61
BS 16084-160	-3.15	4728	1.26	2.1	-0.09	-0.59	155	-0.07	-0.45	137	-0.03	-0.17	105
BS 16545-089	-3.50	6500	4.25	1.6	-0.03	-0.30	27	-0.01	-0.03	21	-0.10	-0.50	16
BS 16550-087	-3.50	4750	1.31	2.3	-0.11	-0.65	122	-0.08	-0.09	105	-0.05	-0.26	78
BS 16928-053	-3.05	4691	1.16	2.1	-0.06	-0.47	69	-0.06	-0.44	61	-0.06	-0.39	48
BS 16929-005	-3.35	5245	2.70	1.6	-0.06	-0.56	97	-0.05	-0.41	83	-0.02	-0.20	63
BS 16467-062	-3.70	5388	3.04	1.7	-0.10	-0.67	52	-0.02	-0.16	41	-0.01	-0.05	34
CS 22872-102	-2.90	5984	3.63	1.5	0.00	-0.02	68	0.00	-0.05	57	0.01	0.06	48
CS 22878-027	-2.50	6348	4.39	1.4	-0.05	-0.52	61	-0.05	-0.39	51	-0.02	-0.13	41
CS 22880-086	-3.00	5188	2.55	1.5	-0.10	-0.70	78	-0.09	-0.58	68	-0.09	-0.56	53
CS 22884-108	-3.15	6290	4.44	1.4	-0.05	-0.33	39	0.00	0.01	31	-0.06	-0.33	24
CS 22944-032	-3.00	5300	2.87	1.5	-0.04	-0.46	124	-0.04	-0.39	112	-0.01	-0.09	86
CS 22957-022	-2.90	5163	2.47	1.6	-0.07	-0.58	125	-0.06	-0.49	114	-0.03	-0.29	88
CS 22963-004	-3.50	5659	3.40	1.6	-0.09	-0.67	60	-0.07	-0.45	49	-0.05	-0.30	36
CS 22965-054	-3.10	6205	3.73	1.7	-0.01	-0.11	44	0.03	0.23	36	0.00	0.01	30
CS 29502-092	-3.30	4890	1.72	1.6	-0.01	-0.11	142	0.00	-0.03	125	0.01	0.13	96
CS 29506-007	-2.85	6369	3.84	1.4	-0.02	-0.25	59	-0.03	-0.22	50	-0.04	-0.27	39
CS 29522-046	-2.10	6055	3.80	1.4	-0.02	-0.27	130	-0.02	-0.23	117	0.00	-0.02	94
CS 30312-059	-3.15	5021	2.06	1.8	-0.05	-0.45	90	-0.04	-0.29	80	-0.02	-0.16	65
CS 30325-028	-2.90	4911	1.70	1.8	-0.07	-0.60	122	-0.06	-0.50	110	-0.03	-0.22	84
CS 30336-049	-3.95	4827	1.51	2.3	-0.13	-0.65	78	-0.11	-0.45	66	-0.01	-0.06	46
CS 31078-018	-2.85	5257	2.75	1.5	-0.07	-0.65	125	-0.07	-0.60	110	-0.03	-0.37	86
CS 31085-024	-2.70	5949	4.57	0.9	-0.07	-0.63	101	-0.06	-0.52	89	-0.04	-0.36	69



TABLE 6  
COMPARISON OF ATMOSPHERIC PARAMETERS

Star ID	This Study			Previous Study			Ref.
	$T_{\text{eff}}$	$\log g$	$v_t$	$T_{\text{eff}}$	$\log g$	$v_t$	
BD+03 740	6557	4.28	1.8	6330	3.55	1.4	1
BD+24 1676	6241	3.81	1.6	6250	3.45	1.2	1
BS 16080-054	4805	1.48	2.1	4800	1.1	2.4	2
BS 16084-160	4728	1.26	2.1	4650	1.1	2.2	2
CS 30312-059	5021	2.06	1.8	4950	2.0	1.8	2
CS 30325-028	4911	1.70	1.8	4900	1.8	2.0	2
BS 16467-062	5388	3.04	1.7	5200	2.5	1.6	3
BS 16467-062	5388	3.04	1.7	5364	2.95	1.6	4

REFERENCES. — (1) Ivans et al. (2003); (2) Aoki et al. (2005); (3) Cayrel et al. (2004); (4) Cohen et al. (2008)

TABLE 7  
ATMOSPHERIC ERRORS FOR BD+03 740

Element	$T_{\text{eff}}$	$\log g$	$v_t$	$\sigma_{\log \epsilon}$	$\sigma_{[X/Fe]}$
	+100 K	+0.2 dex	+0.2 km s <sup>-1</sup>		
Fe I	0.08	0.00	-0.02	0.08	0.00
Fe II	0.02	0.07	0.00	0.05	0.00
Li <sup>1</sup>	0.07	0.00	0.07	0.10	0.09
C	0.13	0.00	-0.05	0.14	0.06
Na <sup>1</sup>	0.07	-0.01	0.07	0.11	0.09
Mg	0.05	-0.02	-0.02	0.07	0.01
Al	0.07	0.00	-0.01	0.07	0.01
Si	0.07	-0.02	-0.06	0.10	0.03
Ca	0.06	0.00	-0.01	0.06	0.02
Sc II	0.05	0.07	-0.01	0.03	0.03
Ti I	0.08	0.01	0.00	0.07	0.02
Ti II	0.05	0.05	-0.03	0.05	0.05
V I	0.08	-0.01	-0.04	0.10	0.02
V II	0.05	0.05	0.00	0.02	0.08
Cr I	0.10	0.00	-0.01	0.10	0.02
Cr II	0.04	0.05	-0.03	0.05	0.04
Mn I	0.09	0.00	-0.01	0.09	0.01
Mn II	0.04	0.05	-0.01	0.02	0.04
Co	0.09	0.01	0.00	0.08	0.01
Ni	0.08	0.00	-0.01	0.08	0.01
Cu	0.11	0.00	0.00	0.11	0.04
Sr II	0.06	0.06	-0.05	0.07	0.07
Y II	0.05	0.06	0.00	0.01	0.05
Zr II	0.06	0.05	-0.01	0.02	0.06
Ba II	0.07	0.06	0.00	0.02	0.07

<sup>1</sup> EWs from CS 22878-027

TABLE 8  
ATMOSPHERIC ERRORS FOR CS 31078-018

Element	$T_{\text{eff}}$ +100 K	$\log g$ +0.2 dex	$v_r$ +0.2 km s <sup>-1</sup>	$\sigma_{\log \epsilon}$	$\sigma_{[X/Fe]}$
Fe I	0.10	-0.02	-0.05	0.03	0.00
Fe II	0.02	0.07	-0.02	0.10	0.00
C	0.20	-0.05	0.00	0.12	0.11
N	0.20	-0.05	0.00	0.12	0.11
O	0.20	-0.10	0.00	0.09	0.14
Na <sup>1</sup>	0.13	-0.05	-0.07	0.08	0.11
Mg	0.09	-0.04	-0.02	0.05	0.09
Al	0.11	-0.03	-0.07	0.04	0.05
Si <sup>2</sup>	0.13	-0.07	-0.05	0.11	0.15
Ca	0.07	0.00	-0.01	0.07	0.03
Sc II	0.05	0.05	-0.03	0.11	0.03
Ti I	0.11	0.00	-0.01	0.11	0.05
Ti II	0.06	0.05	-0.04	0.13	0.03
V I	0.11	0.00	0.00	0.11	0.06
V II	0.06	0.06	-0.01	0.13	0.07
Cr I	0.12	-0.01	-0.06	0.08	0.03
Cr II	0.04	0.03	-0.11	0.13	0.05
Mn I	0.11	-0.02	-0.08	0.05	0.03
Mn II	0.05	0.04	-0.08	0.12	0.03
Co	0.12	0.00	-0.05	0.10	0.04
Ni	0.11	-0.01	-0.08	0.08	0.04
Cu	0.14	-0.01	-0.11	0.11	0.07
Zn	0.04	0.03	0.00	0.08	0.07
Sr II	0.02	0.06	0.00	0.09	0.03
Y II	0.07	0.06	-0.03	0.15	0.03
Zr II	0.07	0.06	-0.02	0.14	0.03
Ru	0.13	0.00	-0.02	0.12	0.07
Pd	0.12	0.00	0.00	0.12	0.07
Ba II	0.12	0.01	-0.16	0.16	0.08
La II	0.07	0.07	-0.01	0.16	0.06
Ce II	0.07	0.07	0.00	0.15	0.06
Nd II	0.07	0.07	0.00	0.15	0.06
Sm II	0.07	0.07	0.00	0.15	0.06
Eu II	0.08	0.07	-0.02	0.17	0.03
Gd II	0.07	0.06	0.00	0.14	0.05
Dy II	0.08	0.06	-0.02	0.15	0.04
Ho II	0.07	0.07	-0.01	0.16	0.06
Er II	0.08	0.07	0.00	0.17	0.07
Yb II	0.10	0.02	-0.17	0.18	0.02

<sup>1</sup> EW from BD+23 3130

<sup>2</sup> EW from BS 16929-005

TABLE 9  
ATMOSPHERIC ERRORS FOR CS 29502-092

Element	$T_{\text{eff}}$ +100 K	$\log g$ +0.2 dex	$v_r$ +0.2 km s <sup>-1</sup>	$\sigma_{\log \epsilon}$	$\sigma_{[X/Fe]}$
Fe I	0.12	-0.03	-0.06	0.09	0.00
Fe II	0.01	0.06	-0.02	0.08	0.00
C	0.25	-0.10	0.00	0.09	0.08
N	0.30	0.00	0.00	0.30	0.22
O	0.25	-0.10	0.00	0.09	0.08
Mg	0.11	-0.05	-0.04	0.01	0.04
Na <sup>1</sup>	0.14	-0.08	-0.09	0.05	0.06
Al	0.12	-0.04	-0.09	0.09	0.03
Si <sup>1</sup>	0.18	-0.08	-0.04	0.02	0.01
Ca	0.07	-0.01	-0.01	0.06	0.04
Sc II	0.06	0.06	-0.02	0.13	0.05
Ti I	0.14	-0.01	-0.01	0.13	0.06
Ti II	0.05	0.06	-0.03	0.13	0.04
V I	0.14	-0.01	-0.01	0.13	0.06
V II	0.06	0.05	-0.02	0.12	0.06
Cr I	0.13	-0.02	-0.03	0.10	0.03
Cr II	-0.02	0.06	0.00	0.03	0.04
Mn I	0.12	-0.01	-0.05	0.12	0.02
Mn II	0.04	0.04	-0.08	0.13	0.05
Co	0.14	-0.02	-0.08	0.13	0.04
Ni	0.11	-0.02	-0.08	0.11	0.02
Cu	0.17	-0.03	-0.10	0.15	0.06
Zn	0.05	0.03	0.00	0.09	0.05
Sr II	0.08	0.03	-0.19	0.24	0.16
Y II	0.08	0.06	-0.01	0.15	0.07
Zr II	0.08	0.06	-0.02	0.16	0.07
Pd	0.17	-0.03	-0.10	0.15	0.06
Cd	0.18	0.01	0.00	0.19	0.11
Ba II	0.08	0.06	-0.02	0.16	0.07
La II <sup>2</sup>	0.08	0.06	-0.01	0.15	0.07
Eu II <sup>2</sup>	0.08	0.06	-0.01	0.15	0.04

<sup>1</sup> EWs from BS 16080-054

<sup>2</sup> EWs from CS 30325-028

TABLE 10  
ABUNDANCES RELATIVE TO FE (AND FE II FOR IONIZED SPECIES)

Star ID	[Fe/H]	numb. lines	$\sigma$ lines	total error	[Fe II/H]	numb. lines	$\sigma$ lines	total error	[C/Fe]	numb. lines	$\sigma$ lines	total error	[N/Fe]	numb. lines	$\sigma$ lines	total error	[O/Fe]	numb. lines	$\sigma$ lines	total error
BD+03 740	-2.71	102	0.10	0.08	-2.69	10	0.10	0.06	0.59	1	0.30	0.31	<0.29	1	...	...	<0.98	1	...	...
BD+23 3130	-2.58	150	0.13	0.03	-2.62	21	0.16	0.11	0.11	1	0.20	0.23	-0.54	1	0.20	0.23	0.55	1	0.30	0.33
BD+24 1676	-2.63	119	0.07	0.08	-2.60	14	0.09	0.06	0.41	1	0.20	0.21	<0.21	1	...	...	0.65	1	0.30	...
BS 16077-007	-2.72	77	0.10	0.08	-2.82	4	0.14	0.09	0.60	1	0.30	0.31	<0.80	1	...	...	<1.39	1	...	...
BS 16080-054	-3.07	91	0.12	0.09	-2.94	11	0.10	0.09	-0.45	1	0.20	0.22	0.75	1	0.30	0.37	...	0	...	...
BS 16080-093	-3.19	94	0.14	0.09	-3.11	12	0.14	0.09	<-0.63	1	...	...	...	0	...	...	...	0	...	...
BS 16084-160	-3.20	155	0.17	0.09	-3.26	16	0.11	0.08	-0.12	1	0.20	0.22	0.78	1	0.20	0.30	0.27	1	0.30	0.31
BS 16467-062	-3.75	52	0.15	0.04	-3.75	3	0.16	0.14	0.48	1	0.20	0.23	...	0	...	...	...	0	...	...
BS 16545-089	-3.44	27	0.06	0.08	-3.44	27	0.06	0.08	<1.62	1	...	...	<1.82	1	...	...	...	0	...	...
BS 16550-087	-3.53	122	0.17	0.09	-3.51	12	0.12	0.09	-0.49	1	0.20	0.22	1.11	1	0.30	0.37	...	0	...	...
BS 16928-053	-3.07	69	0.15	0.09	-3.11	4	0.04	0.08	-0.25	1	0.20	0.22	1.05	1	0.30	0.37	...	0	...	...
BS 16929-005	-3.34	97	0.12	0.03	-3.39	7	0.12	0.11	0.97	1	0.20	0.23	0.32	1	0.30	0.32	...	0	...	...
CS 22872-102	-2.87	68	0.07	0.03	-2.98	4	0.14	0.12	0.60	1	0.20	0.23	<0.55	1	...	...	...	0	...	...
CS 22878-027	-2.48	61	0.11	0.08	-2.68	2	0.08	0.08	0.86	1	0.10	0.12	<1.06	1	...	...	...	0	...	...
CS 22880-086	-3.01	78	0.13	0.03	-3.03	9	0.14	0.11	0.24	1	0.15	0.19	...	0	...	...	...	0	...	...
CS 22884-108	-3.14	39	0.12	0.08	-3.32	2	0.06	0.07	<0.92	1	...	...	<1.22	1	...	...	...	0	...	...
CS 22944-032	-2.98	124	0.11	0.03	-3.04	10	0.09	0.10	0.31	1	0.10	0.15	<-0.44	1	...	...	0.75	1	0.30	0.33
CS 22957-022	-2.93	125	0.13	0.03	-2.92	12	0.10	0.10	0.16	1	0.20	0.23	0.21	1	0.20	0.23	0.60	1	0.30	0.33
CS 22963-004	-3.42	60	0.12	0.03	-3.44	3	0.15	0.13	0.40	1	0.20	0.23	0.80	1	0.20	0.23	0.99	1	0.30	0.33
CS 22965-054	-3.09	44	0.11	0.03	-3.05	4	0.20	0.14	<1.07	1	...	...	...	0	...	...	...	0	...	...
CS 29502-092	-3.18	142	0.09	0.09	-3.20	17	0.12	0.09	0.96	1	0.20	0.22	0.81	1	0.15	0.27	0.75	1	0.30	0.31
CS 29506-007	-2.85	59	0.09	0.08	-2.89	4	0.09	0.07	<0.83	1	...	...	<0.93	1	...	...	<1.52	1	...	...
CS 29522-046	-2.09	130	0.07	0.08	-2.24	18	0.12	0.06	0.42	1	0.20	0.21	-0.33	1	0.30	...	0.66	1	0.20	...
CS 30312-059	-3.14	90	0.12	0.09	-3.19	8	0.05	0.08	0.27	1	0.10	0.13	<-0.48	0	...	...	...	0	...	...
CS 30325-028	-2.90	122	0.14	0.09	-2.96	16	0.11	0.08	0.38	1	0.20	0.22	-0.22	1	0.15	0.27	0.57	1	0.30	0.31
CS 30336-049	-4.04	78	0.18	0.09	-4.16	4	0.10	0.09	-0.28	1	0.30	0.31	0.92	1	0.20	0.30	1.01	1	0.30	0.31
CS 31078-018	-2.84	125	0.12	0.03	-2.91	10	0.13	0.11	0.37	1	0.15	0.19	-0.38	1	0.20	0.23	0.81	1	0.30	0.33
CS 31085-024	-2.68	101	0.12	0.08	-2.71	5	0.13	0.08	0.36	1	0.20	0.21	<-0.24	1	...	...	0.65	1	0.30	...

TABLE 11  
ABUNDANCES RELATIVE TO FE (AND FE II FOR IONIZED SPECIES)

Star ID	[Na/Fe]	numb. lines	$\sigma$ lines	total error	[Mg/Fe]	numb. lines	$\sigma$ lines	total error	[Al/Fe]	numb. lines	$\sigma$ lines	total error	[Si/Fe]	numb. lines	$\sigma$ lines	total error	[Ca/Fe]	numb. lines	$\sigma$ lines	total error
BD+03 740	...	0	...	...	0.23	6	0.04	0.02	-0.84	1	0.15	0.15	0.07	1	0.15	0.15	0.38	11	0.04	0.03
BD+23 3130	-0.09	2	0.08	0.12	0.25	7	0.09	0.10	-0.99	2	0.04	0.06	...	0	...	...	0.24	14	0.09	0.04
BD+24 1676	...	0	...	...	0.37	6	0.07	0.03	...	0	...	...	0.17	1	0.15	0.15	0.45	14	0.08	0.03
BS 16077-007	...	0	...	...	0.34	5	0.08	0.04	...	0	...	...	0.13	1	0.15	0.15	0.43	10	0.03	0.02
BS 16080-054	0.48	2	0.15	0.12	0.44	5	0.09	0.06	-0.70	2	0.04	0.04	0.47	1	0.15	0.15	0.41	11	0.06	0.05
BS 16080-093	...	0	...	...	0.44	8	0.07	0.05	-0.88	2	0.07	0.06	0.42	1	0.15	0.15	0.27	8	0.09	0.05
BS 16084-160	-0.22	2	0.11	0.10	0.21	7	0.07	0.05	-0.97	2	0.04	0.05	0.62	1	0.15	0.15	0.18	10	0.10	0.05
BS 16467-062	...	0	...	...	0.23	4	0.10	0.11	-0.79	2	0.04	0.06	0.32	1	0.15	0.21	0.28	4	0.09	0.06
BS 16545-089	-0.13	1	0.15	0.18	<0.29	1	...	...	-0.66	1	0.15	0.15	0.00	1	0.15	0.15	0.46	1	0.15	0.15
BS 16550-087	0.01	2	0.08	0.08	0.58	9	0.06	0.05	-0.61	2	0.04	0.05	0.40	1	0.15	0.15	0.23	9	0.13	0.06
BS 16928-053	0.03	2	0.08	0.08	0.29	5	0.11	0.07	-0.90	2	0.04	0.05	1.16	1	0.15	0.15	0.21	11	0.08	0.05
BS 16929-005	-0.01	2	0.08	0.12	0.45	7	0.09	0.10	-0.66	2	0.04	0.06	...	0	...	...	0.33	5	0.06	0.04
CS 22872-102	-0.04	2	0.08	0.12	0.38	3	0.09	0.10	-0.72	2	0.11	0.09	0.28	1	0.15	0.21	0.40	13	0.05	0.03
CS 22878-027	-0.28	2	0.17	0.15	0.02	2	0.15	0.11	-0.84	1	0.15	0.15	0.07	1	0.15	0.15	0.18	7	0.18	0.07
CS 22880-086	...	0	...	...	0.29	4	0.08	0.10	-0.97	2	0.08	0.08	...	0	...	...	0.26	4	0.11	0.06
CS 22884-108	...	0	...	...	<0.18	1	...	...	-0.73	2	0.07	0.05	0.11	1	0.15	0.15	0.36	3	0.08	0.06
CS 22944-032	...	0	...	...	0.39	8	0.07	0.09	-0.84	1	0.15	0.16	...	0	...	...	0.29	10	0.06	0.04
CS 22957-022	...	0	...	...	0.28	8	0.09	0.10	...	0	...	...	...	0	...	...	0.22	10	0.07	0.04
CS 22963-004	...	0	...	...	0.35	5	0.06	0.10	-0.85	1	0.15	0.16	0.42	1	0.15	0.21	0.31	3	0.08	0.06
CS 22965-054	...	0	...	...	0.31	2	0.09	0.11	-0.73	1	0.15	0.16	0.08	1	0.15	0.21	0.43	3	0.11	0.07
CS 29502-092	...	0	...	...	0.42	7	0.09	0.05	-0.79	1	0.15	0.15	...	0	...	...	0.31	10	0.10	0.05
CS 29506-007	...	0	...	...	0.28	4	0.10	0.05	-0.82	1	0.15	0.15	0.10	1	0.15	0.15	0.45	5	0.09	0.05
CS 29522-046	...	0	...	...	0.40	5	0.04	0.02	...	0	...	...	...	0	...	...	0.38	14	0.09	0.03
CS 30312-059	0.17	2	0.08	0.08	0.41	5	0.08	0.06	-0.88	2	0.07	0.06	...	0	...	...	0.33	12	0.06	0.05
CS 30325-028	...	0	...	...	0.41	7	0.04	0.04	...	0	...	...	...	0	...	...	0.32	9	0.09	0.05
CS 30336-049	...	0	...	...	0.08	6	0.11	0.06	...	0	...	...	0.19	1	0.15	0.15	0.09	5	0.13	0.07
CS 31078-018	...	0	...	...	0.42	8	0.08	0.09	-0.73	1	0.15	0.16	...	0	...	...	0.41	11	0.10	0.04
CS 31085-024	...	0	...	...	0.17	7	0.07	0.03	...	0	...	...	0.21	1	0.15	0.15	0.22	10	0.07	0.03

TABLE 12  
 ABUNDANCES RELATIVE TO FE (AND FE II FOR IONIZED SPECIES)

Star ID	[ScII/Fe]	numb. lines	$\sigma$ lines	total error	[Ti/Fe]	numb. lines	$\sigma$ lines	total error	[Ti III/Fe]	numb. lines	$\sigma$ lines	total error	[V/Fe]	numb. lines	$\sigma$ lines	total error	[V III/Fe]	numb. lines	$\sigma$ lines	total error
BD+03 740	0.29	4	0.06	0.05	0.69	7	0.07	0.03	0.57	28	0.11	0.06	...	0	...	...	0.28	4	0.06	0.09
BD+23 3130	0.06	6	0.06	0.05	0.21	19	0.06	0.05	0.25	38	0.13	0.05	0.08	3	0.25	0.16	0.12	8	0.09	0.08
BD+24 1676	0.20	5	0.06	0.05	0.55	9	0.08	0.03	0.45	32	0.11	0.06	...	0	...	...	0.20	5	0.09	0.09
BS 16077-007	0.31	3	0.06	0.08	0.59	3	0.10	0.06	0.62	23	0.09	0.07	...	0	...	...	0.42	1	0.15	0.18
BS 16080-054	-0.02	5	0.16	0.09	0.24	6	0.10	0.07	0.30	24	0.10	0.06	...	0	...	...	-0.03	5	0.07	0.07
BS 16080-093	0.09	3	0.06	0.07	0.38	9	0.07	0.07	0.41	28	0.13	0.06	...	0	...	...	-0.09	1	0.15	0.17
BS 16084-160	0.09	6	0.07	0.06	-0.02	11	0.08	0.07	0.09	28	0.09	0.06	...	0	...	...	-0.14	6	0.06	0.07
BS 16467-062	0.31	2	0.06	0.11	0.51	1	0.15	0.16	0.44	9	0.12	0.10	...	0	...	...	...	0	...	...
BS 16545-089	0.29	1	0.15	0.15	...	0	...	...	0.71	10	0.08	0.06	...	0	...	...	...	0	...	...
BS 16550-087	-0.05	4	0.13	0.09	0.18	7	0.13	0.08	0.15	20	0.11	0.07	...	0	...	...	...	0	...	...
BS 16928-053	-0.16	4	0.11	0.08	-0.02	4	0.08	0.07	0.21	16	0.10	0.09	...	0	...	...	-0.37	1	0.15	0.16
BS 16929-005	-0.03	1	0.15	0.16	0.45	6	0.05	0.06	0.50	18	0.13	0.06	...	0	...	...	0.01	1	0.15	0.17
CS 22872-102	0.08	3	0.06	0.08	0.48	3	0.08	0.07	0.42	20	0.13	0.05	...	0	...	...	...	0	...	...
CS 22878-027	0.16	1	0.15	0.16	0.46	2	0.16	0.12	0.53	12	0.12	0.10	...	0	...	...	...	0	...	...
CS 22880-086	0.06	2	0.07	0.07	0.23	4	0.12	0.08	0.36	13	0.10	0.06	...	0	...	...	...	0	...	...
CS 22884-108	0.45	1	0.15	0.16	...	0	...	...	0.80	10	0.12	0.11	...	0	...	...	...	0	...	...
CS 22944-032	0.11	3	0.11	0.08	0.32	13	0.09	0.06	0.36	25	0.12	0.05	...	0	...	...	0.16	5	0.04	0.08
CS 22957-022	0.05	3	0.06	0.06	0.30	8	0.06	0.06	0.33	26	0.08	0.05	-0.09	1	0.15	0.16	0.04	5	0.04	0.08
CS 22963-004	0.27	2	0.06	0.10	...	0	...	...	0.44	17	0.12	0.08	...	0	...	...	0.07	1	0.15	0.19
CS 22965-054	0.03	1	0.15	0.18	...	0	...	...	0.42	10	0.12	0.07	...	0	...	...	...	0	...	...
CS 29502-092	0.02	6	0.04	0.06	0.18	19	0.08	0.06	0.19	27	0.12	0.05	-0.06	2	0.16	0.13	0.04	6	0.02	0.07
CS 29506-007	0.28	2	0.08	0.08	0.66	2	0.08	0.06	0.57	20	0.13	0.07	...	0	...	...	...	0	...	...
CS 29522-046	0.12	5	0.04	0.04	0.35	14	0.07	0.03	0.43	32	0.12	0.06	0.06	1	0.15	0.15	0.17	6	0.06	0.09
CS 30312-059	0.07	3	0.06	0.06	0.31	5	0.07	0.07	0.39	17	0.10	0.06	...	0	...	...	0.04	5	0.04	0.07
CS 30325-028	0.08	5	0.09	0.07	0.26	19	0.08	0.06	0.35	32	0.12	0.06	-0.11	1	0.15	0.16	0.03	5	0.05	0.07
CS 30336-049	0.18	4	0.07	0.08	0.16	1	0.15	0.16	0.27	22	0.12	0.10	...	0	...	...	...	0	...	...
CS 31078-018	0.10	4	0.06	0.06	0.31	11	0.07	0.06	0.38	26	0.09	0.05	0.06	2	0.16	0.13	0.13	5	0.04	0.08
CS 31085-024	0.14	2	0.07	0.08	0.32	4	0.08	0.05	0.38	22	0.16	0.08	...	0	...	...	0.14	3	0.05	0.10

TABLE 13  
 ABUNDANCES RELATIVE TO FE (AND FE II FOR IONIZED SPECIES)

Star ID	[Cr/Fe]	numb. lines	$\sigma$ lines	total error	[Cr II/Fe]	numb. lines	$\sigma$ lines	total error	[Mn/Fe]	numb. lines	$\sigma$ lines	total error	[Mn II/Fe]	numb. lines	$\sigma$ lines	total error	[Co/Fe]	numb. lines	$\sigma$ lines	total error
BD+03 740	-0.07	5	0.05	0.03	0.05	2	0.10	0.09	-0.46	3	0.16	0.09	-0.19	3	0.06	0.06	0.41	3	0.09	0.05
BD+23 3130	-0.24	19	0.10	0.04	-0.07	4	0.16	0.10	-0.57	10	0.13	0.05	-0.38	3	0.07	0.06	0.20	2	0.16	0.12
BD+24 1676	-0.13	7	0.09	0.04	-0.09	3	0.12	0.08	-0.43	5	0.21	0.09	-0.30	3	0.06	0.06	0.35	2	0.09	0.06
BS 16077-007	-0.15	6	0.06	0.03	0.01	2	0.10	0.11	-0.52	3	0.16	0.09	-0.27	2	0.06	0.09	0.34	2	0.09	0.06
BS 16080-054	-0.43	7	0.26	0.10	-0.21	1	0.15	0.16	-0.61	4	0.25	0.13	-0.59	1	0.15	0.16	0.08	3	0.09	0.07
BS 16080-093	-0.34	5	0.13	0.07	...	0	...	...	-0.98	3	0.16	0.10	...	0	...	...	0.30	2	0.10	0.08
BS 16084-160	-0.42	10	0.16	0.06	...	0	...	...	-0.55	9	0.25	0.09	-0.44	3	0.06	0.07	0.09	3	0.11	0.08
BS 16467-062	-0.46	4	0.11	0.06	...	0	...	...	-0.64	3	0.16	0.10	...	0	...	...	0.69	3	0.09	0.07
BS 16545-089	-0.15	1	0.15	0.15	...	0	...	...	...	0	...	...	...	0	...	...	...	0	...	...
BS 16550-087	-0.59	4	0.16	0.09	...	0	...	...	-0.96	3	0.16	0.10	...	0	...	...	0.22	3	0.09	0.07
BS 16928-053	-0.25	4	0.11	0.06	...	0	...	...	-0.71	4	0.24	0.12	-0.50	2	0.12	0.10	0.04	3	0.11	0.08
BS 16929-005	-0.50	4	0.11	0.06	...	0	...	...	-0.80	3	0.16	0.10	...	2	0.10	0.09	0.38	3	0.09	0.06
CS 22872-102	-0.32	5	0.08	0.05	...	0	...	...	-0.62	3	0.16	0.10	-0.44	3	0.10	0.10	0.22	3	0.09	0.06
CS 22878-027	-0.12	5	0.06	0.04	...	0	...	...	-0.34	3	0.16	0.09	-0.04	1	0.15	0.17	...	0	...	...
CS 22880-086	-0.37	2	0.11	0.08	...	0	...	...	-0.50	4	0.27	0.14	...	0	...	...	0.47	3	0.09	0.07
CS 22884-108	-0.25	4	0.11	0.06	...	0	...	...	-0.50	2	0.16	0.11	...	0	...	...	...	0	...	...
CS 22944-032	-0.31	9	0.10	0.05	...	0	...	...	-0.44	6	0.21	0.09	-0.19	3	0.06	0.05	0.45	3	0.09	0.06
CS 22957-022	-0.30	9	0.13	0.05	...	0	...	...	-0.76	3	0.16	0.10	-0.25	3	0.06	0.05	0.29	3	0.13	0.09
CS 22963-004	-0.40	5	0.08	0.05	...	0	...	...	-0.77	3	0.16	0.10	-0.42	1	0.15	0.18	0.48	2	0.09	0.07
CS 22965-054	-0.05	3	0.11	0.07	...	0	...	...	-0.30	2	0.16	0.12	...	0	...	...	0.26	1	0.15	0.16
CS 29502-092	-0.21	15	0.12	0.04	0.21	2	0.10	0.08	-0.32	8	0.26	0.09	-0.16	3	0.06	0.07	0.36	3	0.09	0.06
CS 29506-007	-0.17	6	0.08	0.04	...	0	...	...	-0.69	3	0.16	0.09	-0.42	1	0.15	0.16	0.28	1	0.15	0.15
CS 29522-046	-0.12	15	0.06	0.03	0.11	3	0.12	0.08	-0.47	7	0.16	0.06	-0.27	3	0.06	0.06	0.17	3	0.09	0.05
CS 30312-059	-0.34	6	0.20	0.09	0.09	1	0.15	0.16	-0.88	3	0.16	0.10	-0.53	3	0.06	0.06	0.28	3	0.09	0.07
CS 30325-028	-0.26	15	0.10	0.04	-0.01	2	0.10	0.08	-0.51	6	0.28	0.12	-0.41	3	0.17	0.11	0.23	3	0.12	0.08
CS 30336-049	-0.74	5	0.16	0.08	...	0	...	...	-0.82	3	0.16	0.10	-0.52	2	0.07	0.09	0.47	3	0.10	0.07
CS 31078-018	-0.31	6	0.11	0.06	-0.18	1	0.15	0.16	-0.20	6	0.20	0.09	0.01	3	0.06	0.06	0.34	3	0.16	0.10
CS 31085-024	-0.23	7	0.07	0.04	-0.10	1	0.15	0.17	-0.41	5	0.23	0.10	-0.19	3	0.06	0.08	0.37	3	0.09	0.05

TABLE 14  
ABUNDANCES RELATIVE TO FE (AND FE II FOR IONIZED SPECIES)

Star ID	[Ni/Fe]	numb. lines	$\sigma$ lines	total error	[Cu/Fe]	numb. lines	$\sigma$ lines	total error	[Zn/Fe]	numb. lines	$\sigma$ lines	total error	[Sr II/Fe]	numb. lines	$\sigma$ lines	total error	[Y II/Fe]	numb. lines	$\sigma$ lines	total error
BD+03 740	0.06	3	0.08	0.05	-0.80	2	0.06	0.06	...	0	...	...	-0.21	2	0.06	0.09	-0.01	1	0.15	0.16
BD+23 3130	-0.15	5	0.10	0.06	-1.33	2	0.14	0.12	0.07	2	0.04	0.08	-0.38	2	0.10	0.08	-0.39	11	0.08	0.05
BD+24 1676	0.03	4	0.08	0.04	-0.83	2	0.06	0.06	0.20	1	0.15	0.18	-0.05	2	0.05	0.08	-0.12	5	0.05	0.06
BS 16077-007	0.08	3	0.08	0.05	-0.59	1	0.15	0.16	...	0	...	...	0.22	2	0.05	0.11	0.30	1	0.15	0.17
BS 16080-054	-0.05	3	0.11	0.07	...	0	...	...	...	0	...	...	0.16	2	0.05	0.17	0.12	8	0.14	0.09
BS 16080-093	0.03	2	0.14	0.10	...	0	...	...	...	0	...	...	-0.13	2	0.05	0.17	-0.28	4	0.09	0.09
BS 16084-160	-0.13	4	0.13	0.07	-1.64	2	0.11	0.10	...	0	...	...	-2.10	2	0.11	0.18	...	0	...	...
BS 16467-062	0.29	2	0.08	0.07	...	0	...	...	...	0	...	...	...	0	...	...	...	0	...	...
BS 16545-089	...	0	...	...	...	0	...	...	...	0	...	...	-0.09	2	0.07	0.09	...	0	...	...
BS 16550-087	-0.08	3	0.10	0.06	...	0	...	...	...	0	...	...	0.42	2	0.05	0.17	0.29	9	0.09	0.08
BS 16928-053	-0.15	2	0.08	0.06	...	0	...	...	...	0	...	...	-0.34	2	0.05	0.17	-0.41	5	0.12	0.09
BS 16929-005	0.08	3	0.09	0.07	...	0	...	...	...	0	...	...	0.37	2	0.08	0.08	0.22	4	0.09	0.07
CS 22872-102	0.03	3	0.10	0.07	...	0	...	...	...	0	...	...	-0.15	2	0.05	0.09	...	0	...	...
CS 22878-027	0.06	3	0.08	0.05	...	0	...	...	...	0	...	...	-0.18	2	0.05	0.10	...	0	...	...
CS 22880-086	0.16	3	0.08	0.06	...	0	...	...	...	0	...	...	-0.10	2	0.05	0.07	-0.27	3	0.15	0.10
CS 22884-108	0.00	2	0.11	0.08	...	0	...	...	...	0	...	...	0.29	2	0.10	0.11	...	0	...	...
CS 22944-032	0.10	4	0.08	0.06	-1.10	2	0.06	0.08	0.25	1	0.15	0.17	-0.27	2	0.10	0.08	-0.30	7	0.07	0.05
CS 22957-022	-0.02	3	0.11	0.08	-1.23	2	0.07	0.09	0.31	2	0.04	0.08	-0.41	1	0.15	0.16	-0.37	6	0.11	0.06
CS 22963-004	0.08	2	0.08	0.07	-0.94	2	0.07	0.09	...	0	...	...	-0.80	2	0.05	0.10	...	0	...	...
CS 22965-054	0.00	2	0.08	0.07	...	0	...	...	...	0	...	...	0.06	2	0.05	0.11	...	0	...	...
CS 29502-092	0.08	5	0.07	0.04	-1.36	2	0.11	0.10	0.34	2	0.04	0.06	-0.46	2	0.07	0.17	-0.63	8	0.06	0.08
CS 29506-007	-0.06	2	0.08	0.06	< -0.56	1	...	...	...	0	...	...	0.13	2	0.06	0.09	0.24	1	0.15	0.16
CS 29522-046	-0.03	5	0.10	0.05	-0.79	2	0.06	0.06	0.15	2	0.05	0.11	0.22	2	0.06	0.09	0.09	8	0.05	0.06
CS 30312-059	-0.05	3	0.10	0.06	...	0	...	...	...	0	...	...	-0.02	2	0.06	0.17	-0.01	6	0.09	0.08
CS 30325-028	-0.04	4	0.09	0.05	-1.18	2	0.06	0.07	0.33	2	0.09	0.08	0.16	3	0.15	0.18	0.01	12	0.06	0.08
CS 30336-049	-0.05	2	0.08	0.06	-1.17	1	0.15	0.16	...	0	...	...	-1.50	2	0.10	0.18	...	0	...	...
CS 31078-018	0.09	4	0.10	0.06	-1.02	2	0.07	0.09	0.41	1	0.15	0.17	0.24	1	0.15	0.16	0.24	10	0.08	0.06
CS 31085-024	0.21	3	0.08	0.05	-0.93	2	0.06	0.06	...	0	...	...	-0.30	2	0.05	0.10	...	0	...	...



TABLE 15  
ABUNDANCES RELATIVE TO FE (AND FE II FOR IONIZED SPECIES)

Star ID	[Zr II/Fe]	numb. lines	$\sigma$ lines	total error	[Ba II/Fe]	numb. lines	$\sigma$ lines	total error	[La II/Fe]	numb. lines	$\sigma$ lines	total error	[Eu II/Fe]	numb. lines	$\sigma$ lines	total error
BD+03 740	0.36	2	0.11	0.10	-0.37	1	0.15	0.17	...	0	...	...	<0.68	1	...	...
BD+23 3130	0.00	10	0.12	0.06	-0.47	3	0.06	0.09	-0.26	1	0.15	0.17	0.31	1	0.10	0.11
BD+24 1676	0.31	5	0.14	0.09	-0.33	2	0.06	0.09	...	0	...	...	<0.59	1	...	...
BS 16077-007	0.85	2	0.19	0.16	-0.11	1	0.15	0.18	...	0	...	...	<0.81	1	...	...
BS 16080-054	0.31	9	0.19	0.10	-0.42	4	0.06	0.08	...	0	...	...	<0.23	1	...	...
BS 16080-093	0.17	1	0.15	0.17	-0.27	2	0.06	0.09	...	0	...	...	0.20	1	0.20	0.21
BS 16084-160	...	0	...	...	-1.99	2	0.09	0.10	...	0	...	...	<-0.25	1	...	...
BS 16467-062	...	0	...	...	<-0.68	1	...	...	...	0	...	...	<1.24	1	...	...
BS 16545-089	...	0	...	...	<-0.09	1	...	...	...	0	...	...	<1.93	1	...	...
BS 16550-087	0.74	8	0.16	0.10	-0.74	4	0.15	0.11	...	0	...	...	<0.00	1	...	...
BS 16928-053	-0.10	2	0.14	0.12	-0.82	4	0.10	0.09	...	0	...	...	<-0.40	1	...	...
BS 16929-005	0.53	2	0.11	0.10	-0.28	3	0.06	0.10	...	0	...	...	<0.03	1	...	...
CS 22872-102	...	0	...	...	-0.45	1	0.15	0.18	...	0	...	...	<1.07	1	...	...
CS 22878-027	...	0	...	...	<-0.75	1	...	...	...	0	...	...	<1.17	1	...	...
CS 22880-086	...	0	...	...	-0.80	2	0.06	0.10	...	0	...	...	<0.22	1	...	...
CS 22884-108	...	0	...	...	0.24	1	0.15	0.17	...	0	...	...	<1.91	1	...	...
CS 22944-032	0.05	5	0.06	0.05	-0.62	2	0.06	0.09	...	0	...	...	<0.73	1	...	...
CS 22957-022	-0.05	3	0.11	0.08	-1.01	2	0.06	0.10	...	0	...	...	<-0.09	1	...	...
CS 22963-004	...	0	...	...	-0.44	1	0.15	0.19	...	0	...	...	<1.43	1	...	...
CS 22965-054	...	0	...	...	<-0.48	1	...	...	...	0	...	...	<1.14	1	...	...
CS 29502-092	-0.28	5	0.05	0.08	-1.26	2	0.06	0.09	...	0	...	...	<-0.31	1	...	...
CS 29506-007	0.63	3	0.11	0.10	0.11	1	0.15	0.17	...	0	...	...	<0.88	1	...	...
CS 29522-046	0.41	9	0.11	0.08	0.14	3	0.06	0.08	...	0	...	...	<0.23	1	...	...
CS 30312-059	0.35	7	0.11	0.08	-0.01	4	0.06	0.08	...	0	...	...	0.63	1	0.10	0.11
CS 30325-028	0.40	19	0.11	0.08	-0.34	3	0.06	0.08	-0.18	1	0.15	0.17	0.15	1	0.20	0.21
CS 30336-049	...	0	...	...	-1.32	1	0.15	0.17	...	0	...	...	<0.95	1	...	...
CS 31078-018	0.63	16	0.09	0.06	0.72	3	0.27	0.18	0.74	1	0.15	0.17	1.23	4	0.04	0.05
CS 31085-024	...	0	...	...	-0.52	1	0.15	0.18	...	0	...	...	<0.60	1	...	...

TABLE 16  
NEUTRON-CAPTURE ABUNDANCES OF CS  
31078-018

Atomic Number	Element Name	[X/Fe]	$\log\epsilon(X)$	error
38	Sr II	0.31	0.30	0.18
39	Y II	0.23	-0.43	0.15
40	Zr II	0.62	0.32	0.14
44	Ru I	0.65	-0.35	0.19
46	Pd I	0.79	-0.36	0.19
56	Ba II	0.72	-0.06	0.31
57	La II	0.74	-1.00	0.22
58	Ce II	0.66	-0.67	0.21
60	Nd II	0.79	-0.62	0.21
62	Sm II	1.13	-0.77	0.16
63	Eu II	1.23	-1.17	0.17
64	Gd II	1.03	-0.76	0.17
66	Dy II	1.00	-0.77	0.15
67	Ho II	1.54	-1.11	0.22
68	Er II	1.02	-0.96	0.20
70	Yb II	0.76	-1.07	0.21
90	Th II	1.47	-1.35	0.25

TABLE 17  
A SAMPLE OF HIGHLY NEUTRON-CAPTURE DEFICIENT  
STARS

Star ID	[Fe/H]	[Sr/H]	[Ba/H]	source
BS 16084-160	-3.26*	-5.29	-5.25	1
CS 30336-049	-4.16*	-5.59	-5.48	1
CS 29502-092	-3.20*	-3.59	-4.46	1
HD 4306	-2.89	-3.00	-4.06	2
BS 16469-075	-3.03	-2.80	-4.15	2
BS 16920-017	-3.12	-3.55	-4.95	2
BS 16928-053	-2.91	-3.14	-4.07	2
Draco 119	-2.97	< -5.47	< -5.57	3
CS 22169-035	-3.04	-3.12	-4.23	4
CS 22172-002	-3.86	-5.17	-5.03	4
CS 22189-009	-3.49	-4.44	-4.78	4
CS 22897-008	-3.41	-2.97	-4.41	4
CS 22952-015	-3.43	-4.42	-4.76	4
CS 22968-014	-3.56	-5.36	-5.33	4
CS 29502-042	-3.19	-5.17	-4.88	4
CS 30325-094	-3.30	-5.54	-5.21	4
BS 16934-002	-2.81*	-4.13	-4.61	5
CS 30327-038	-2.64*	-3.28	-4.14	5
HE 1356-0622	-3.36*	-5.24	-4.45	5

REFERENCES. — (1) This study; (2) Honda et al. (2004); (3) Fulbright et al. (2004); (4) François et al. (2007); (5) Aoki et al. (2005); (6) Cohen et al. (2008)

\* [Fe II/H]

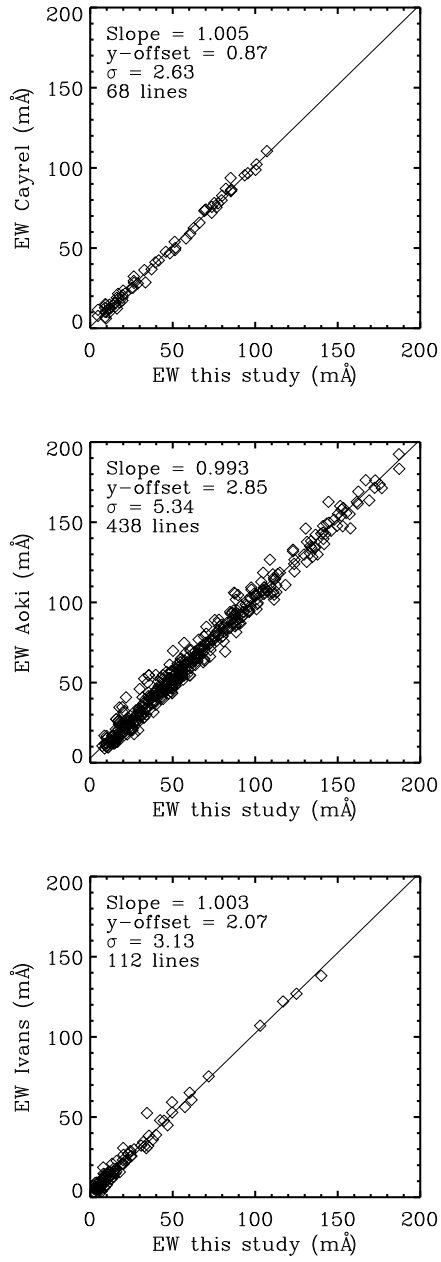


FIG. 1.— The top panel compares the EWs measured by Cayrel et al. (2004) with our study, the middle panel shows the comparison with Aoki et al. (2005), and the bottom panel shows the comparison with Ivans et al. (2003).

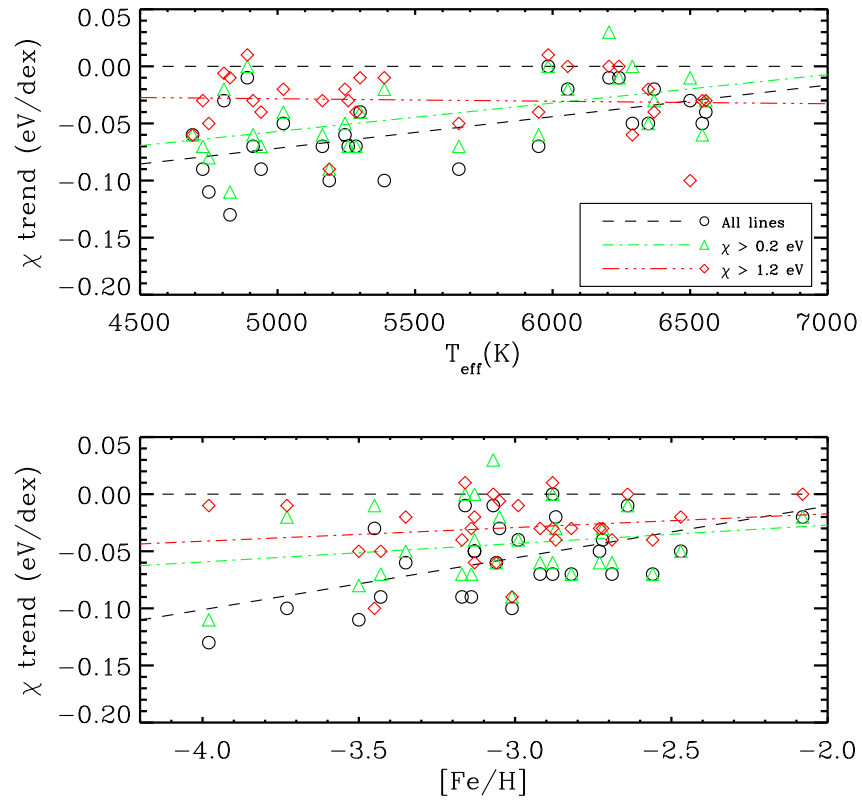


FIG. 2.— Value of the  $\chi/\log\epsilon(\text{Fe I})$  slopes for each of our stars. When all Fe I lines are considered, there seems to be a trend with both  $T_{\text{eff}}$  and  $[\text{Fe}/\text{H}]$ , although considering only the  $\chi > 1.2$  eV lines, this trend largely disappears. Overall, however, even when considering high  $\chi$  lines, we still seem to be finding a negative slope in most of our stars. See the electronic edition of the Journal for a color version of this figure.

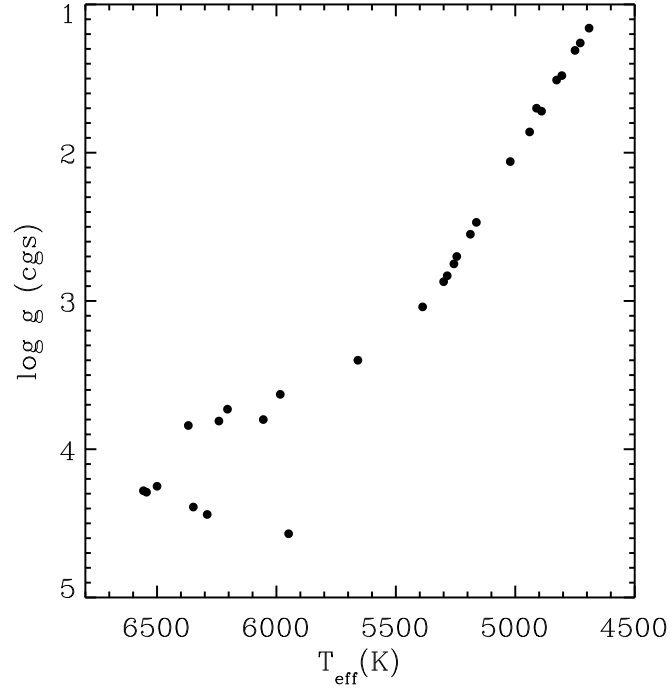


FIG. 3.— Plot of  $T_{\text{eff}}$  vs.  $\log g$  for our stars. The sample spans a wide range of evolutionary states.

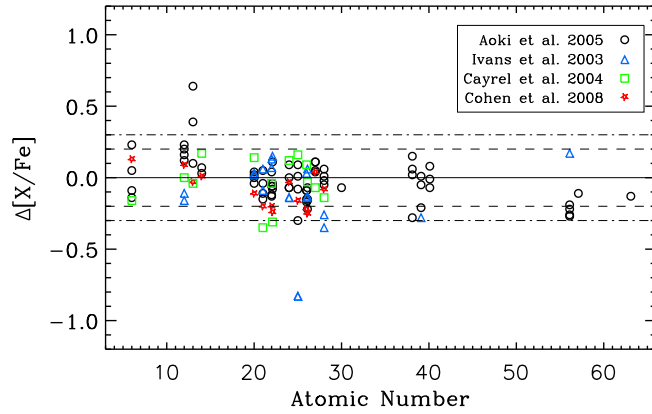


FIG. 4.— Comparison of our abundance to that of other studies. The sense of the y-axis is the values from this study minus the values from previous studies. See the electronic edition of the Journal for a color version of this figure.

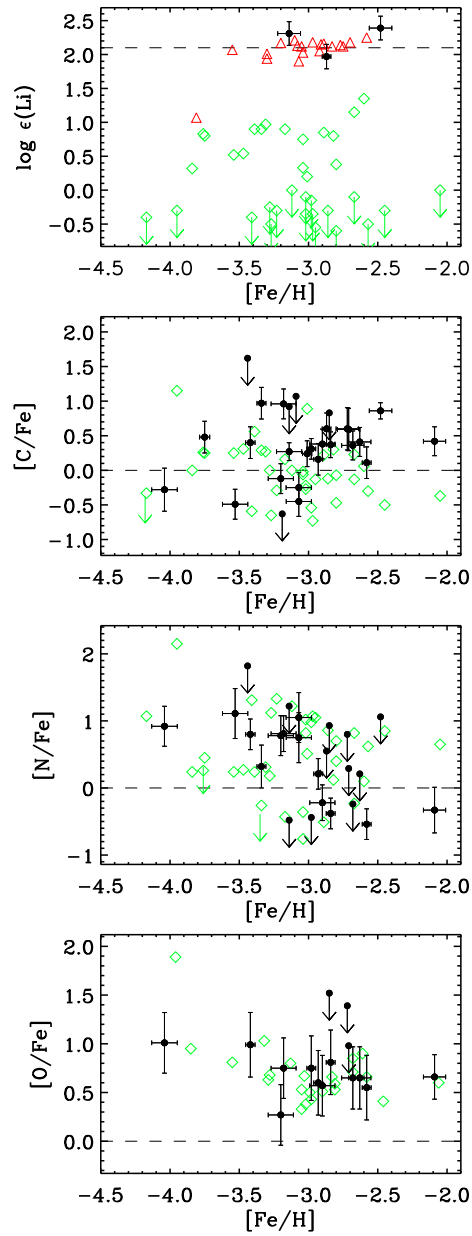


FIG. 5.— Values of  $\text{Log}\epsilon(\text{Li})$  and  $[(\text{C},\text{N},\text{O})/\text{Fe}]$  vs.  $[\text{Fe}/\text{H}]$ . The diamonds (colored green in the electronic edition) are from Spite et al. (2005) and the triangles (colored red in the electronic edition) are from Bonifacio et al. (2007). In all of the following figures, the black points with error bars are data from this study. See the electronic edition of the Journal for a color version of this figure.

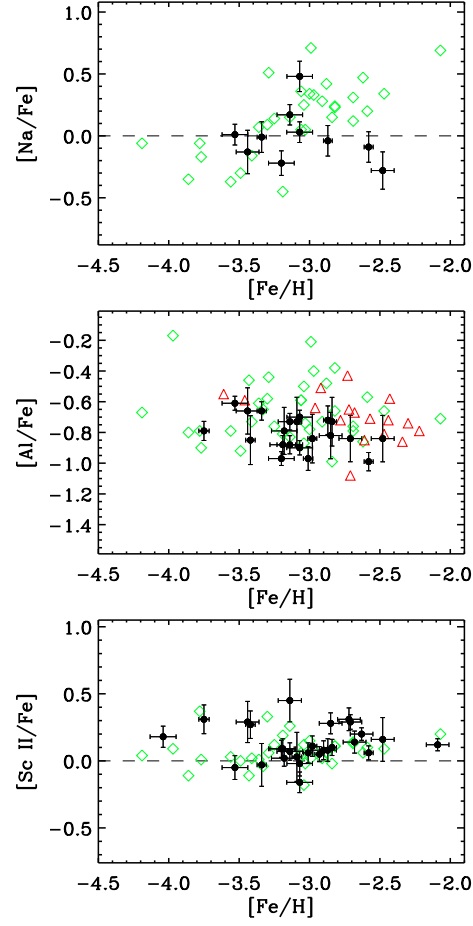


FIG. 6.—  $[(Na,Al,Sc)/Fe]$  vs.  $[Fe/H]$ . The diamonds (colored green in the electronic edition) are from Cayrel et al. (2004) and the triangles (colored red in the electronic edition) are from Cohen et al. (2004). Although we only have two stars below  $[Fe/H]$  of  $-2.7$  with measured Na, we do not find the trend found by Cayrel et al. (2004). The  $[Al/Fe]$  values from Cohen et al. (2004) are plotted without the NLTE correction of 0.6 dex assumed in that study. See the electronic edition of the Journal for a color version of this figure.

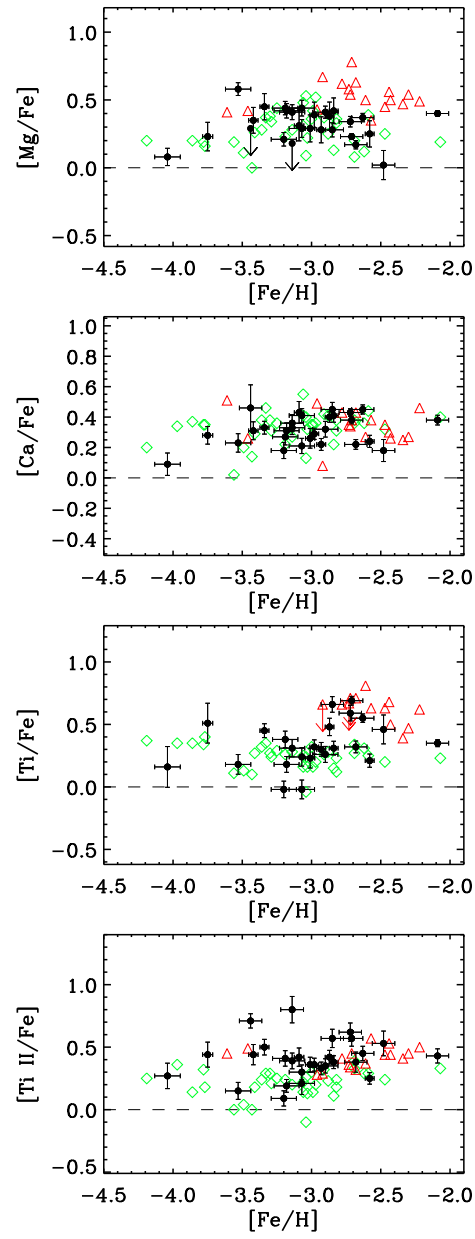


FIG. 7.—  $[\alpha/\text{Fe}]$  vs.  $[\text{Fe}/\text{H}]$ . The symbols are as in figure 6. See the electronic edition of the Journal for a color version of this figure.



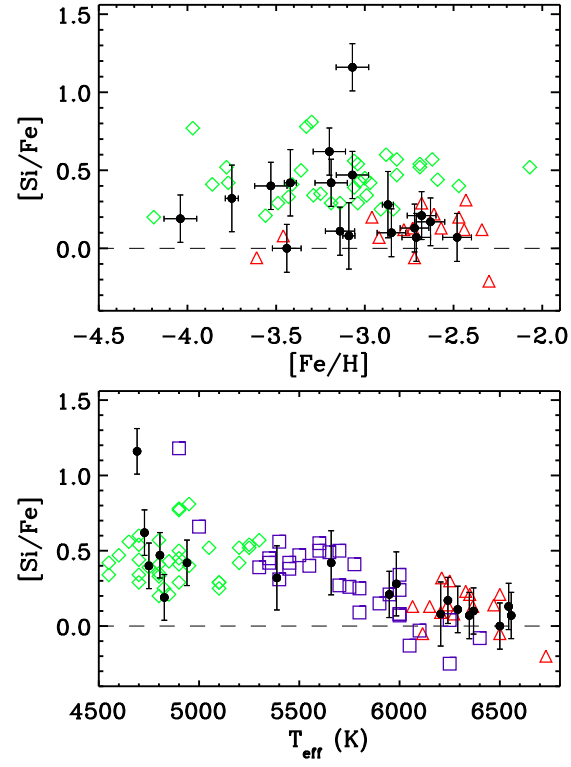


FIG. 8.—  $[\text{Si}/\text{Fe}]$  vs.  $[\text{Fe}/\text{H}]$  and  $T_{\text{eff}}$ . The symbols are as in figure 6. In the bottom panel, we also add the data from Preston et al. (2006) as the squares (colored purple in the electronic edition). See the electronic edition of the Journal for a color version of this figure.

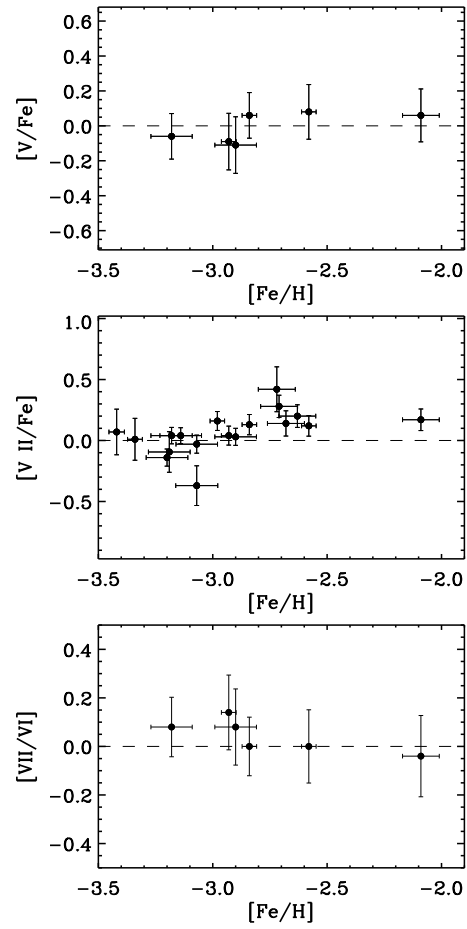


FIG. 9.— Vanadium abundance vs.  $[Fe/H]$ . We plot both the neutral and singly ionized species, along with  $[V II/V I]$ . We find no offset between the  $V II$  and  $V I$  abundances.

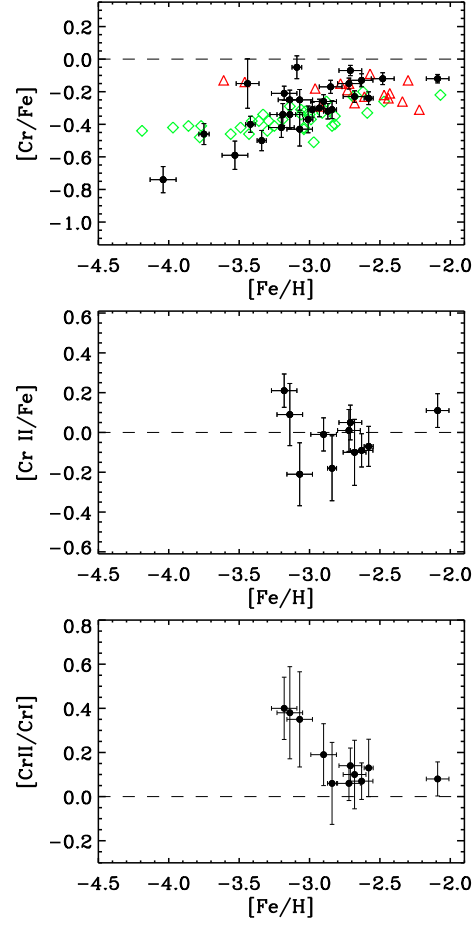


FIG. 10.— Cr abundance vs.  $[Fe/H]$ . We plot both the neutral and singly ionized species, along with  $[Cr II/Cr I]$ . The symbols are as in figure 6. Although we do not measure Cr II for many of our stars, our results suggest an offset from zero for  $[Cr II/Cr I]$ , as well as an increasing trend in this value with decreasing metallicity. See the electronic edition of the Journal for a color version of this figure.

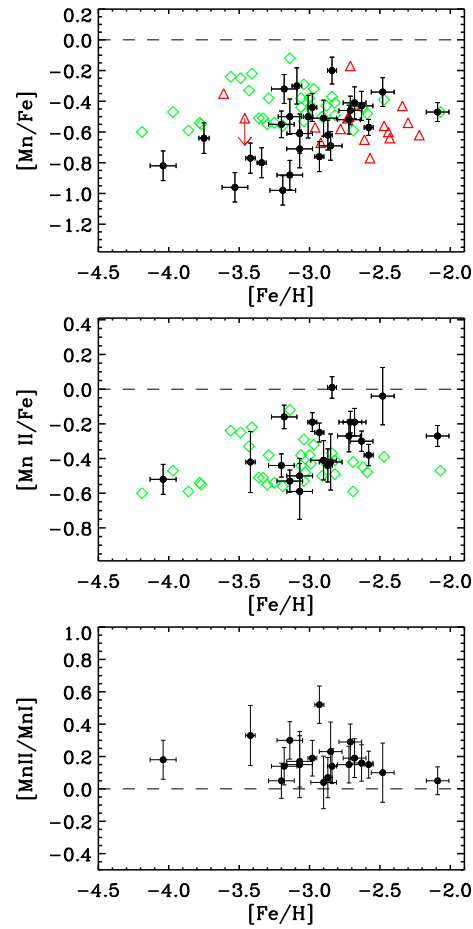


FIG. 11.— Manganese abundance vs.  $[Fe/H]$ . We plot both the neutral and singly ionized species, along with  $[Mn II/Mn I]$ . The symbols are as in figure 6. In the  $[Mn II/Fe]$  plot, we also overplot the  $[Mn/Fe]$  values from Cayrel et al. (2004) for the reasons described in the text. See the electronic edition of the Journal for a color version of this figure.

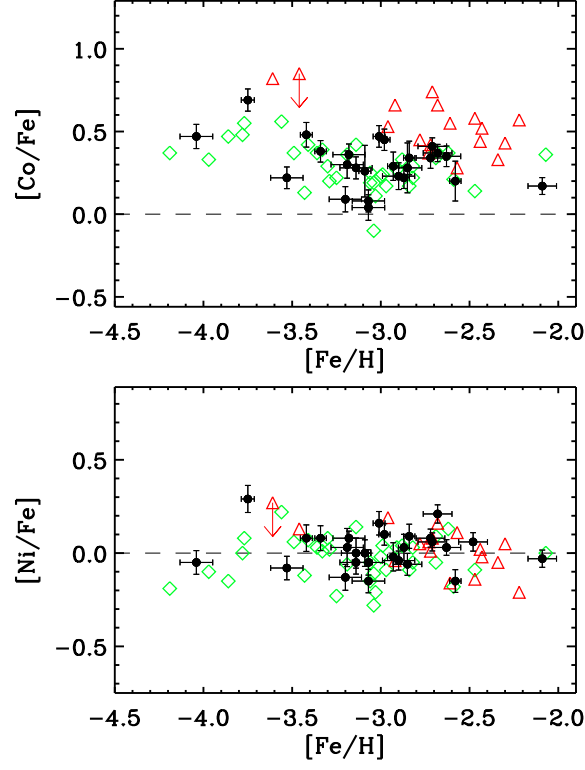


FIG. 12.—  $[\text{Co}, \text{Ni}/\text{Fe}]$  vs.  $[\text{Fe}/\text{H}]$ . The symbols are as in figure 6. We find a similar trend of increasing  $[\text{Co}/\text{Fe}]$  with decreasing  $[\text{Fe}/\text{H}]$  as in Cayrel et al. (2004). The  $[\text{Ni}/\text{Fe}]$  shows no trend with  $[\text{Fe}/\text{H}]$ . See the electronic edition of the Journal for a color version of this figure.

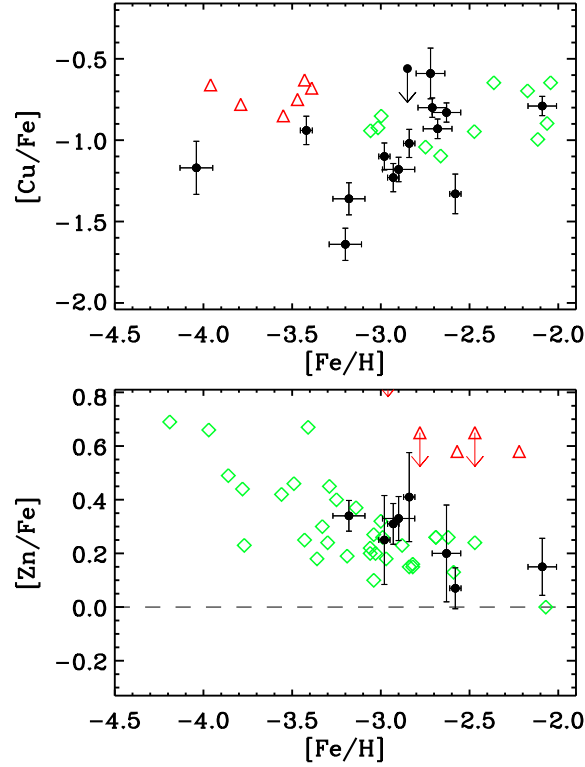


FIG. 13.—  $[(\text{Cu}, \text{Zn})/\text{Fe}]$  vs.  $[\text{Fe}/\text{H}]$ . The triangles (colored red in the electronic edition) in the  $[\text{Cu}/\text{Fe}]$  plot are from Cohen et al. (2008), and the diamonds (colored green in the electronic edition) are from Bihain et al. (2004). In the  $[\text{Zn}/\text{Fe}]$  plot, the symbols are as in figure 6. See the electronic edition of the Journal for a color version of this figure.

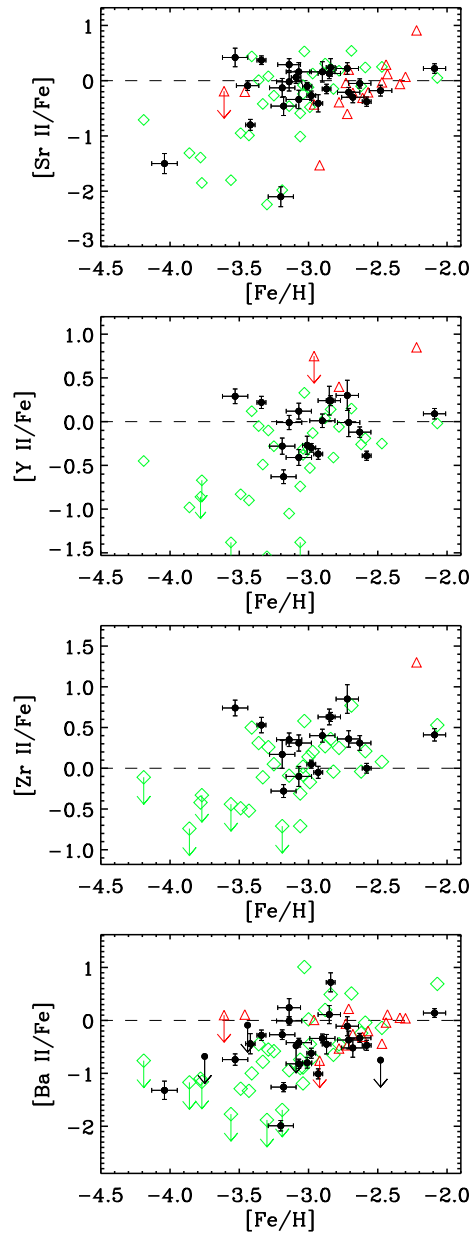


FIG. 14.—  $[(\text{Sr II}, \text{Y II}, \text{Zr II}, \text{Ba II})/\text{Fe}]$  vs.  $[\text{Fe}/\text{H}]$ . We clearly see a large scatter in all of these abundances. The triangles (colored red in the electronic edition) are from Cohen et al. (2008) and the diamonds (colored green in the electronic edition) are from François et al. (2007). See the electronic edition of the Journal for a color version of this figure.

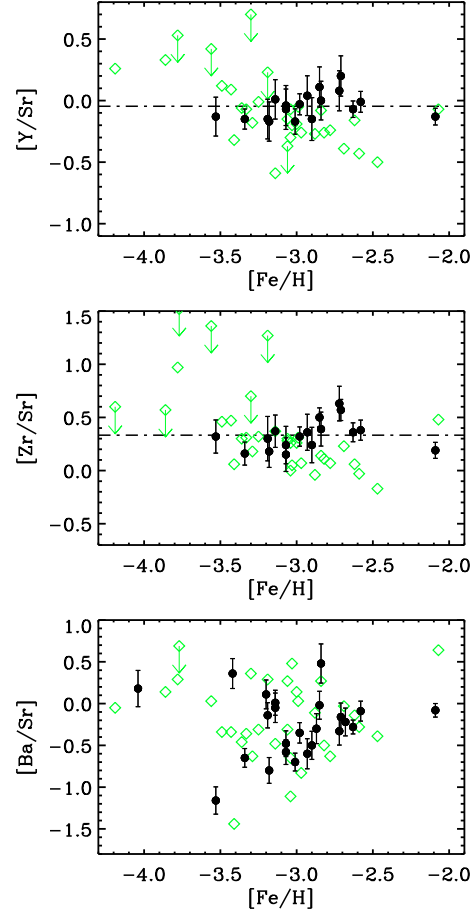


FIG. 15.— The light neutron-capture elements, Sr, Zr, and Y, show remarkable correlation, while  $[\text{Sr}/\text{Ba}]$  shows a scatter of almost 2 dex. The diamonds (colored green in the electronic edition) are from François et al. (2007). See the electronic edition of the Journal for a color version of this figure.

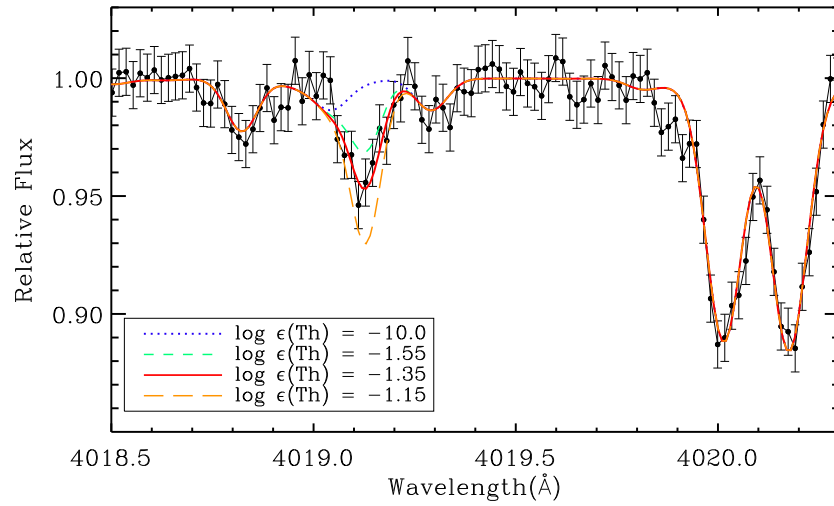


FIG. 16.— Spectral synthesis of the Th line at 4019 Å in CS 31078-018. See the electronic edition of the Journal for a color version of this figure.

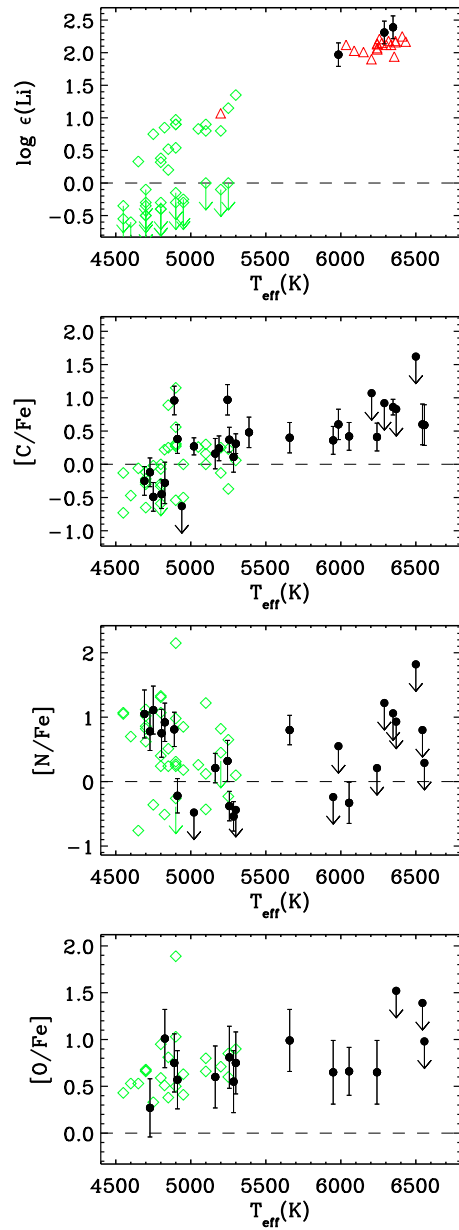


FIG. 17.— Values of  $\log \epsilon(\text{Li})$  and  $[\text{C}, \text{N}, \text{O}/\text{Fe}]$  vs.  $T_{\text{eff}}$ . The symbols are as in figure 5. See the electronic edition of the Journal for a color version of this figure.



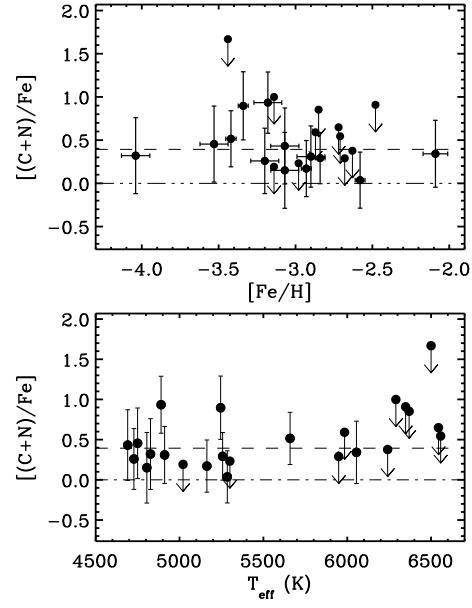


FIG. 18.—  $[(C+N)/Fe]$  vs.  $[Fe/H]$  and  $T_{\text{eff}}$ . The large number of upper limits obscures any potential trend with  $[Fe/H]$ ; however, it seems clear that  $[(C+N)/Fe]$  is not correlated with  $T_{\text{eff}}$ . The rms scatter for the measured  $[C+N/Fe]$  is 0.27 dex, and the average value is 0.39 dex.

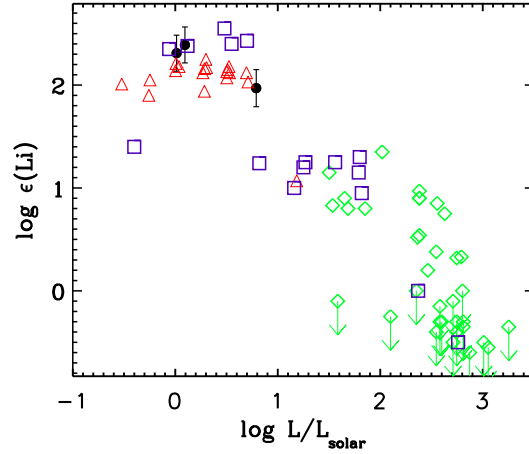


FIG. 19.— Values of  $\log \epsilon(Li)$  vs. luminosity. The symbols are as in figure 5, with the addition of the squares (colored purple in the electronic edition) from Gratton et al. (2000). See the electronic edition of the Journal for a color version of this figure.

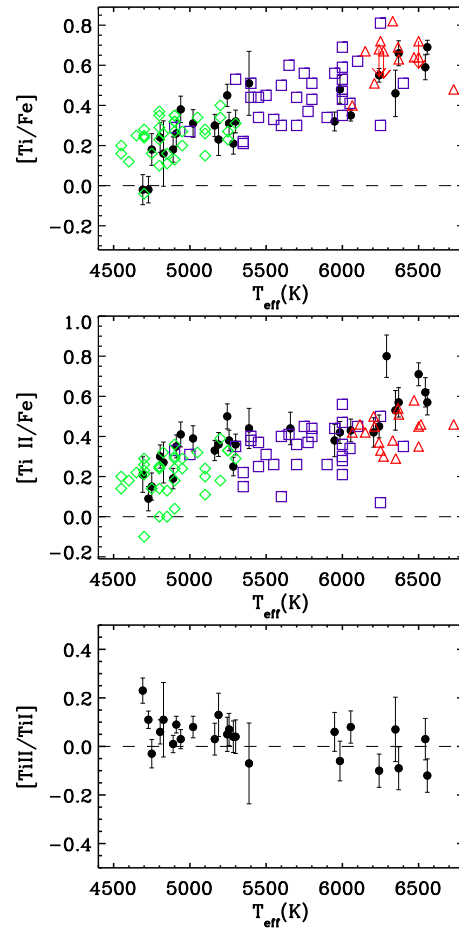


FIG. 20.—  $[\text{Ti}/\text{Fe}]$  and  $[\text{Ti II}/\text{Fe}]$  versus  $T_{\text{eff}}$ . We also plot  $[\text{Ti II}/\text{Ti I}]$ , which shows that, although there is an offset between these values, the trend exists for both the neutral and singly ionized states. We also plot data taken from Preston et al. (2006) as the squares (colored purple in the electronic edition). See the electronic edition of the Journal for a color version of this figure.

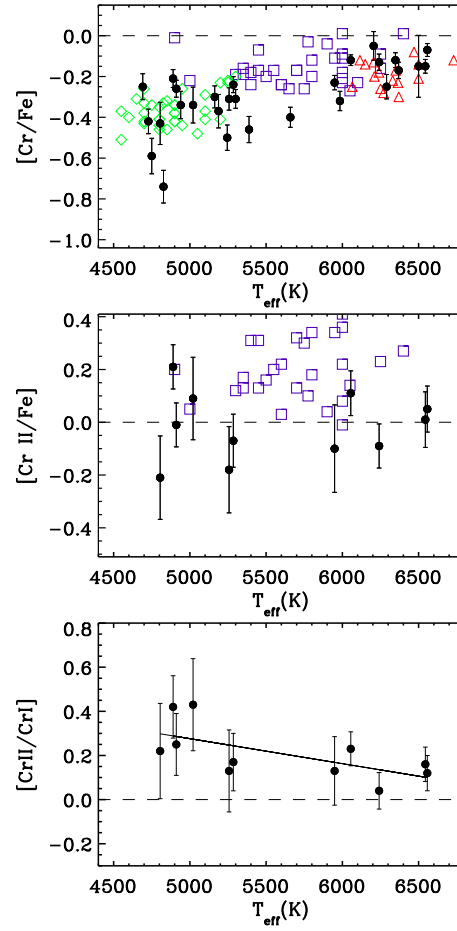


FIG. 21.—  $[\text{Cr}/\text{Fe}]$  and  $[\text{Cr II}/\text{Fe}]$  vs.  $T_{\text{eff}}$ . We also plot  $[\text{Cr II}/\text{Cr I}]$ , which shows that although there is an offset between these values, the trend exists for both the neutral and singly ionized states. The symbols are as in figure 20.

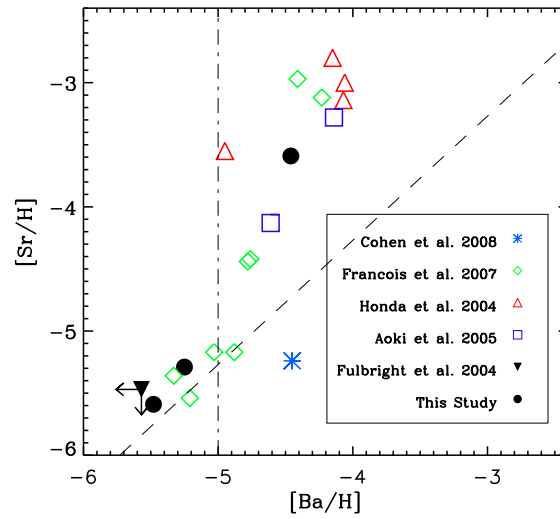


FIG. 22.—  $[\text{Sr}/\text{H}]$  vs.  $[\text{Ba}/\text{H}]$ . In these neutron-capture deficient objects, it seems that there are at least two sites that produce  $[\text{Sr}/\text{H}]$ . The main  $r$ -process line, as given in Simmerer et al. (2004) is plotted as the dashed line. See the electronic edition of the Journal for a color version of this figure.

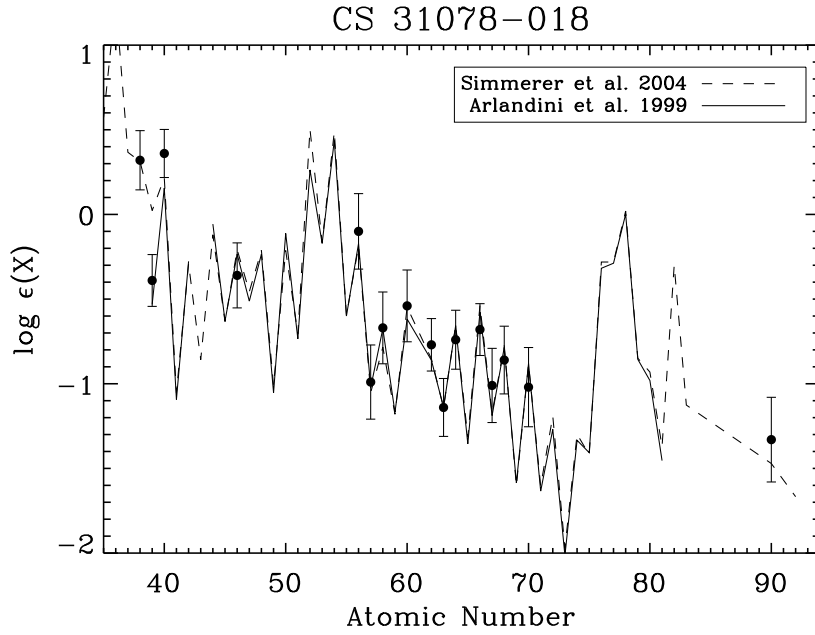


FIG. 23.— Measured neutron-capture elements in the star CS 31078-018. The solar system  $r$ -process lines come from Arlandini et al. (1999) and Simmerer et al. (2004), and have been scaled to match our Eu abundance.

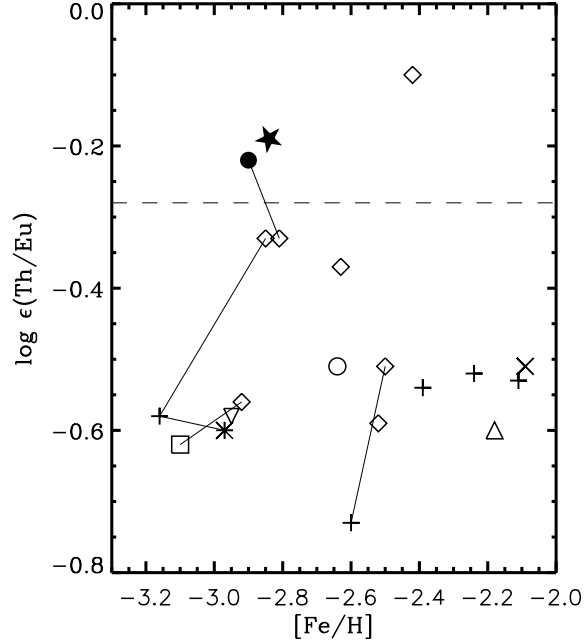


FIG. 24.— Measured  $\log \epsilon(\text{Th}/\text{Eu})$  abundances of metal-poor stars. The symbols represent the following: the filled star is CS 31078-018 from this study, the diamonds are stars from Honda et al. (2004), the plus signs are stars from Johnson & Bolte (2001), the solid circle is CS 31082-001 from Hill et al. (2002), the upward-pointing triangle is HD 221170 from Ivans et al. (2006), the downward-pointing triangle is HE 1523-0901 from Frebel et al. (2007a), the square is CS 22892-052 from Sneden et al. (2003), the cross is BD+17 3248 from Cowan et al. (2002), the open circle is CS 29497-004 from Christlieb et al. (2004), and the asterisk is HD 115444 from Westin et al. (2000). The solid lines connect points that are repeated measurements of the same object. Honda et al. (2004) suggest that the discrepancy in the measurements for HD 115444 arise from a combination of differing atmospheric parameters and linelists. There is a clear distribution of values, although a majority of the stars have  $\log \epsilon(\text{Th}/\text{Eu}) \sim -0.6$ . The production ratio from Kratz et al. (2007) is plotted as the dashed line.

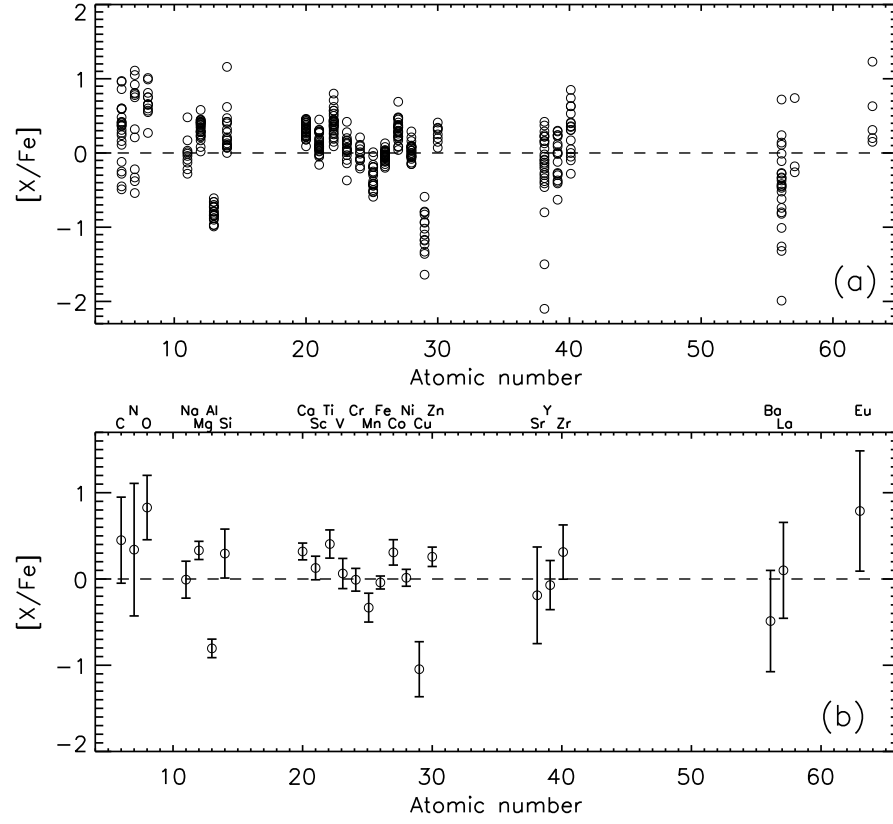


FIG. 25.— Abundance spread of our sample. When both the ionized and neutral species of an element are measured, we plot only the results for the ionized species. The points plotted for Fe are the Fe II - Fe I values of our stars. (a) Here we plot all of our measurements for the sample from C through Eu. (b) Instead of all of the measurements, we show the average measured abundance for each element. The error bars represent the rms of the abundances of each respective element.

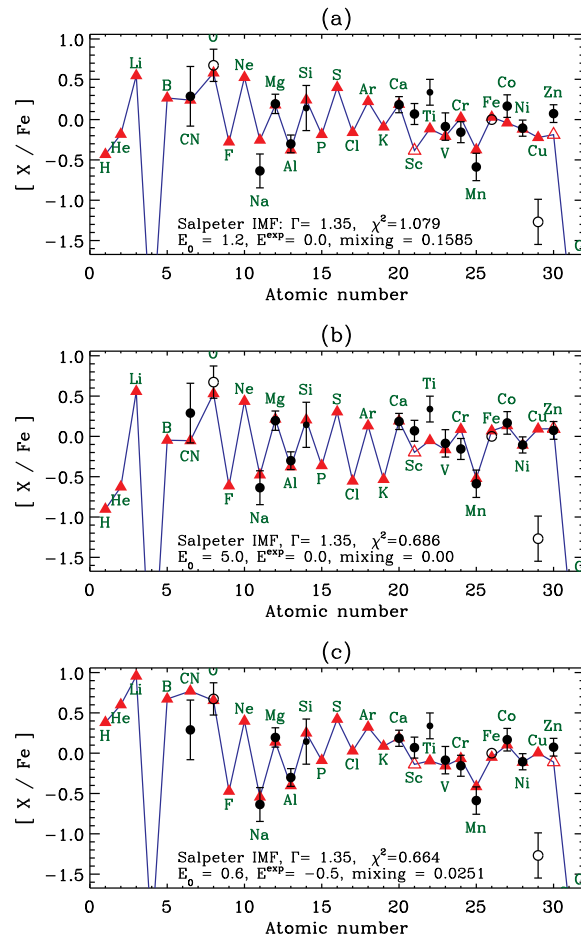


FIG. 26.— Average abundance pattern of our sample fitted to the Heger & Woosley (2008) models assuming a Salpeter IMF. The filled circles are the averaged abundances, with the error bars corresponding to the rms of the abundance ratios over our sample. The smaller filled circles of Si and Ti represent the smaller weights attributed to them in the fitting procedure. The open circles are when that particular abundance is not used in the fit, and the open triangles at Sc and Zn represent treating the model yields as lower limits.

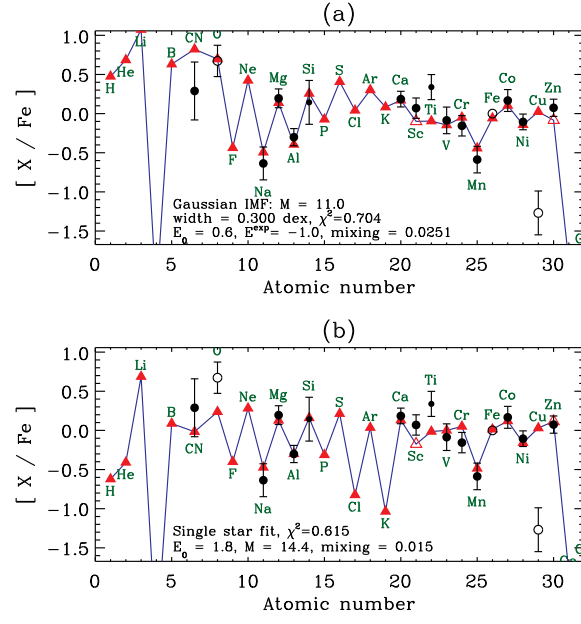


FIG. 27.— Average abundance pattern of our sample fitted to the Heger & Woosley (2008) models. The symbols are as in Fig. 26. (a) Best fit assuming a Gaussian IMF. (b) Best fit to a single SN.

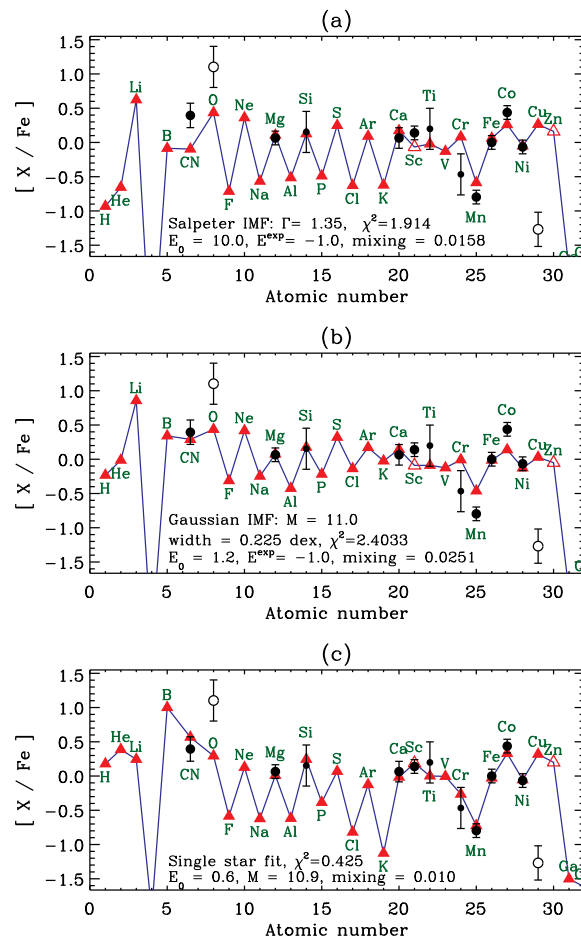


FIG. 28.— Abundance pattern of CS 30336-049 fitted to the Heger & Woosley (2008) models. Oxygen and copper are ignored, and the Cr has been increased by 0.3 dex. The type of fit and its parameters are listed on each plot.



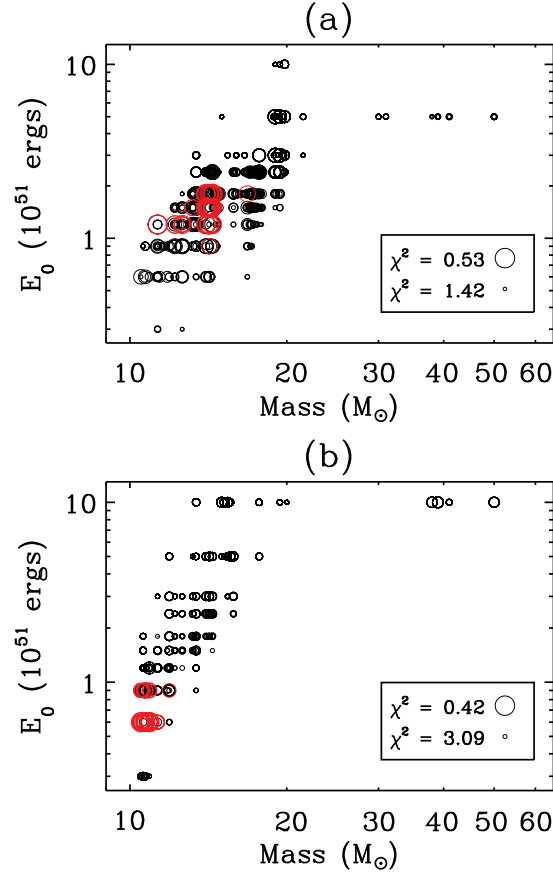


FIG. 29.— The 1000 best-fit single explosion models to (a) our average abundance pattern and (b) CS 30336-049. The  $\chi^2$  values are represented linearly by the size of the circles, with the minimum and maximum  $\chi^2$  of the fits shown in the legends of each respective plot. Mixing values are not differentiated in these plots. The best 50 fits for each case are plotted in red.

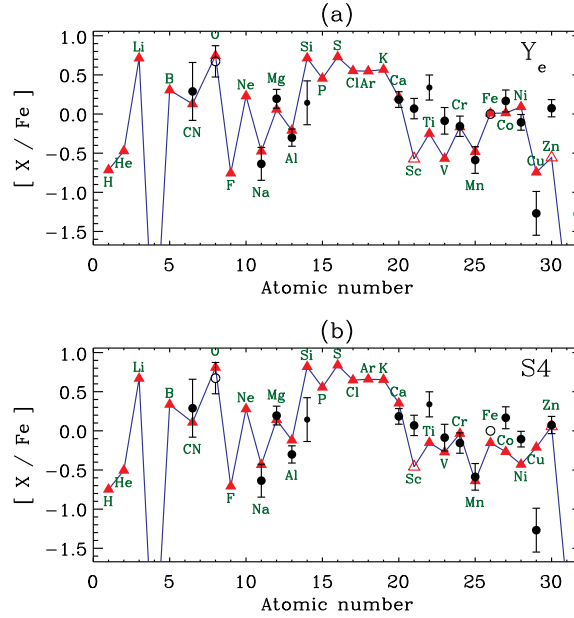


FIG. 30.— Plot of the effect of positioning the piston at the  $Y_e$  boundary (edge of the iron core) and the S4 ( $S/N_A k = 4.0$ ) boundary (base of the convective shell). The black points with error bars again represent the average abundance pattern of our sample. (a) Best single star fit assuming a piston location at the edge of the iron core. (b) Model with the same parameters, but with the piston location at the base of the convective shell.